Journal Pre-proof

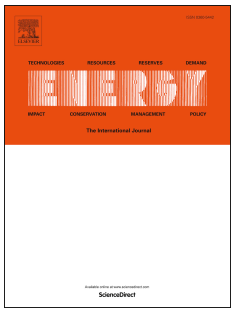

A comprehensive exergy evaluation of a deep borehole heat exchanger coupled with a ORC plant: The case study of Campi Flegrei

Alimonti C, Conti P, Soldo E

PII: S0360-5442(19)31795-5

DOI: https://doi.org/10.1016/j.energy.2019.116100

Reference: EGY 116100

To appear in: *Energy*

Received Date: 9 January 2019

Revised Date: 24 August 2019

Accepted Date: 8 September 2019

Please cite this article as: C A, P C, E S, A comprehensive exergy evaluation of a deep borehole heat exchanger coupled with a ORC plant: The case study of Campi Flegrei, *Energy* (2019), doi: https://doi.org/10.1016/j.energy.2019.116100.

A comprehensive exergy evaluation of a deep borehole heat exchanger coupled with a ORC plant: the case study of Campi Flegrei

Alimonti C[1], Conti P[2], Soldo E[1]

[1]University of Rome – DICMA, Via Eudossiana 18, 00184 ROMA

[2]University of Pisa – DESTEC, Largo Lucio Lazzarino - 56122 Pisa

Abstract

The paper presents a comprehensive energy and exergy analysis of a possible geothermal power plant located in the geothermal district of Campi Flegrei (Italy), made of a coaxial WellBore Heat eXchanger coupled to an Organic Rankine Cycle. We have accounted for all system components: the ground source, the WellBore Heat eXchanger, the Organic Rankine Cycle cycle, and cooling system. The energy and exergy performance indexes of each subsystems and overall system have been evaluated, thus calculating the net power, the First-Law efficiency, the Second-law efficiency, the irreversibilities. The results indicate a good potential of the WellBore Heat eXchanger – Organic Rankine Cycle technology in the area, as the estimated performances have similar values to those of classical binary geothermal power plants: a First-Law efficiency of 11.67% and a Second-Law efficiency of about 43.80%. The overall system performances decrease respectively to 10.62% due to the fans energy requirements in the cooling tower and to 23.15% due to the large exergy destruction occurring in the WellBore Heat eXchanger. A deep exergy analysis of the WellBore Heat eXchanger has highlighted that the overall irreversibility is strongly affected by the insulation performance between the two coaxial pipes and by the temperature deviation between the ground and the fluid. The latter one is mainly due to the continuous heat extraction from the geothermal source, therefore proposed improvement strategies consist of both the increasing of thermal resistance of the material insulating the upward pipe and the reduction of the equivalent thermal radius of the well optimizing the heat extraction profiles over the plant lifetime.

Keywords

Geothermal energy, WellBore heat exchanger, Organic Rankine Cycle, exergy analysis, Campi Flegrei, optimized design.

Nomenclature

a	thermal diffusivity	[m^2/s]
c	specific heat capacity	[J/kg K]
D_h	hydraulic diameter	[m]
$\dot{ex}$	specific exergy	[kJ/kg]
$\dot{Ex}$	exergy rate	[W]
gradT	temperature gradient	[°C/100 m]

$\dot{H}$	enthalpy	[W]
h	specific enthalpy	[kJ/kg]
$\dot{I}$	exergy destruction	[W]
k	convective heat transfer	[W/m^2 K]
L	total length of the well	[m]
$\dot{m}$	mass flow rate	[kg/s]
P	power output	[W]
p	pressure	[bar, MPa]
$\dot{Q}$	total thermal power	[W]
$\dot{q}$	heat flux	[W/m^2]
ρ	density	[kg/m^3]
R	thermal resistance	[mK/W]
r	radius	[mm]
s	specific entropy	[kJ/kgK]
T	temperature	[K or °C]
t	time	[s]
u	velocity	[m/s]
$\dot{W}$	mechanical/electrical power	[W]
Z	depth	[m]

Greek symbols

η	efficiency	
λ	thermal conductivity	[W/m K]
ξ	friction factor	
ρ	density	[kg/m^3]

Subscripts, superscripts

a	ambient state
CP	circulation pump
CT	cooling tower
DSH+COND	desuperheater + condenser

dw	downward
el	electrical
em	electrical-mechanical
EVA	evaporator
f	fluid
HX	heat-exchanger
I	first-law
II	second-law
i	inner
in	inlet
o	outer
ORC	organic ranking cycle
out	outlet
P	pump
PH	preheater
s	soil property
SH	superheater
sys	overall system
T	turbine
up	upward
w	water
wCT	water in the cooling tower
wf	working fluid
WBHX	WellBore Heat eXchanger
WP	WBHX pump
0	reference state

1. Background and motivations

The use of ORC technology for geo-power production (i.e. binary power plants) has become an established solution worldwide. At the end of 2014, the geothermal sector counted 279 binary units (46% of the geothermal world total) for an installed capacity of about 1700 MW_{el} (14% of the

geothermal word total) (Bertani 2016). Since 2000, several researches have been focused on the possibility to produce geothermal energy through ORC systems, but without brine extraction, using a deep borehole heat exchanger, named WellBore Heat eXchanger (WBHX) by Nalla et al. (2005). The device is made of two coaxial tubes inserted into the well: in the external annulus is injected a heat carrier fluid which is heated going deep; at the bottomhole the fluid enters in the internal tube and it flows up to the wellhead (Figure 1). The final use of the extracted heat can be the production of thermal power or electricity with an Organic Rankine Cycle (ORC) plant (Alimonti and Soldo, 2018). The WellBore Heat eXchanger has been applied only in two abandoned wells in Switzerland, at Weggis and at Weissbad (Kohl et al., 2002).

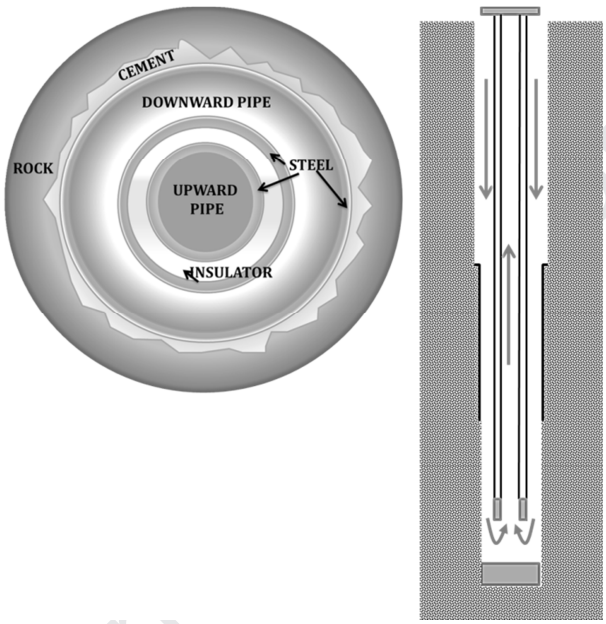

Figure 1 – The wellBore Heat eXchanger.

1.1 The research on the WellBore Heat eXchanger

The study of the performance of the WBHX is widely treated in literature, focusing the analysis on the operational parameters, design characteristics, thermal properties of the formation and the heat carrier fluid. The results obtained by the researches indicate that the key parameter of the heat extraction with the WBHX is the residence time of the fluid in the device, which is function of flow rate and diameters. At fixed design, there is a specific value of the flow rate that guarantees the maximum outlet temperature. At fixed flow rate the residence time is function of the WBHX diameters (Wang et al., 2009; Alimonti and Soldo, 2016); therefore, the optimization of energy production requests the study of the more appropriate design.

It has been demonstrated that the insulation of the internal pipe is necessary in order to avoid heat exchange between the hotter and the colder fluid (Kohl et al., 2002; Nalla et al., 2006; Kujawa et al., 2006; Wang et al., 2009). The insulation can be realized for the entire length or for a limited length (Kujawa et al., 2006; Alimonti and Soldo, 2016); regarding the material, the compressed air (Alimonti and Soldo, 2016), the magnesia (Nalla et al., 2006) and the polystyrene have been proposed (Davis and Michaelides, 2009).

The temperature of the extracted fluid is directly proportional to the geothermal gradient, the thermal conductivity and the volumetric heat capacity of the formation (Nalla et al., 2006; Bu et al., 2012; Cheng et al., 2013; Templeton et al., 2014; Le Lous et al., 2015; Noorollahi et al., 2015).

Concerning the working fluid, two different solutions have been followed: some authors suggest circulating a heat carrier fluid in the WBHX and a low boiling point fluid in the ORC plant, other

authors propose a unique working fluid (iso-pentane, iso-butane, R134a and R245fa) for the coupled WBHX-ORC plant. The heat transfer in the WBHX is related to the volumetric heat capacity of the selected fluid and, according to the results of Nalla et al. (2006) and Alimonti and Soldo (2016), the water is the most efficient heat carrier fluid.
Some authors have studied different design solutions in order to increase the efficiency of the WBHX, such as a high inlet temperature (Templeton et al., 2014), a partial insulation of the external casing (Wang et al., 2009), a limited cased and cemented length (Nalla et al., 2006), the fracturing of the rock and the use of high conductivity material to fill the fractures (Taleghani et al., 2015), the use of an external annulus where the brine is pumped (Akhmadullin and Tyagi, 2014; Feng et al., 2015).
The low mass flow rate that circulates in the device and the heat exchange mainly by conduction are responsible of the low efficiency in heat recovery respect to the conventional geothermal plants. The analysis of literature indicates a maximum wellhead temperature of 150 °C, a range of produced thermal power of 0.15÷2.5 MW and a range of 0.25÷364 kW for the electricity.

Anyway, the possibility to produce geothermal heat without brine extraction is quite interesting because this technological solution avoids the risks of corrosion and scaling of the pipes, groundwater pollution, land subsidence and micro-seismicity. Therefore, some authors (Galoppi et al., 2015; Alimonti et al., 2016) evaluated the application of the WBHX in unconventional geothermal systems, in which the brine is absent or it requests special and expensive treatments.

1.2 Exergy analysis of geothermal WellBore Heat eXchanger systems: state of the art

The exergy, also called available work, is a measure of to the maximum work output that could theoretically be obtained from any system interacting with a given environment which is at constant pressure and temperature (p_a, T_a) (Di Pippo 2004; Ozgener et al., 2004, Kotas 1995). According to Kestin (1980), the first formulation of exergy concept is by J.W. Gibbs (1878). The exergy analysis evaluates the irreversible production of entropy; therefore, it is useful to identify both maximum theoretical performances and the inefficiencies of a system and its components.

According to DiPippo (2015) and Zarrouk (2014), the exergy analysis is now a standard methodology to assess the energy conversion performance of geothermal ORC systems and to identify those elements within a plant that are most ineffective. The first analysis of a geothermal plant based on exergy concept was carried out by Bodvarrson and Eggers (1972). Then Lee (2001) proposed a classification of geothermal resources based on exergy; the author has developed the “specific exergy index” (SExI), a normalized parameter with values between 0 and 1. The method of Lee was applied to classify the geothermal resources of Turkey (Etemoglou and Can, 2007), of Poland (Barbacki, 2012) and of Japan (Jalilinasrabady and Itoi, 2013). Ramajo et al. (2010) proposed a modification of SExI tool to evaluate how the exploitation influences the geothermal resources and their characteristics in the future; Coskun et al. (2009) developed some energetic and exergetic parameters to analyze a geothermal district heating system in Balikesir, Turkey. Several authors have used the exergy to evaluate the efficiency of a real geothermal power plant or district heating plant (Quijano, 2000; Ozgener et al., 2004; Ozgener et al., 2005; Baba et al., 2006; Jalilinasrabady et al. 2012; Ganjehsarabi et al. 2012; Ahmadi et al. 2016; Gökgedik et al. 2016; Koroneos et al. 2017). Other papers are focused on the exergy analysis of different type of geothermal plants: Di Pippo (2004) evaluated some existing binary plants; Yari (2008) has applied the energetic and exergetic analysis to single-flash power plant, double-flash power plant, flash-binary power plant, binary power plant; Fallah et al. (2018) have compared different types of geothermal plants (dry steam, flash cycles, binary plants) from exergy and thermo-economic point of view.

About 50 papers are available in literature regarding the deep borehole heat exchanger, but only two of them (Feng et al., 2015; Mokhtari et al., 2016) include a thermodynamic assessment of the Organic Rankin Cycle based on the energy and exergy balances. Nevertheless, both the studies do not account for the energy losses due to the cooling of the condenser (i.e., the cooling tower). Moreover, the WBHX model proposed by Mokhtari et al., (2016) assumes the ground in a stationary condition, neglecting the effect of the heat extraction on the source temperature. On the contrary, the plant operation alters the natural temperature gradient of the soil, reducing the source temperature and increasing the equivalent thermal resistance of the well, which strongly reduces the sustainability of the heat transfer process.

In this paper, we present a comprehensive energy and exergy analysis of a possible WBHX - ORC power plant located in a real (still undeveloped) geothermal area in Italy: the Campi Flegrei, We account for all system components: the ground source, the WBHX, the ORC cycle, and cooling system (i.e., the cooling towers). We aim at investigating the second-law thermodynamic efficiency of each subsystem in order to figure out their influence on the final power production efficiency. Additionally, the exergy efficiency quantifies the deviation from the ideal maximum performance. The identification of the most critical components is also functional to address future research activities as we might identify rooms for improvement and upper limits at both components and system level for the WBHX - ORC technology.

2. The case study: Campi Flegrei

The Campi Flegrei area has a typical horseshoe shape and is located in the north-west limit of the Napoli gulf; the area is a caldera of 12 km with the centre in the Pozzuoli bay (Figure 2). The area is part of the Neapoletan volcanoes district, which includes also Ischia island and Somma-Vesuvius volcano. This large area is characterized by thermal manifestations (hot springs, fumaroles, gas emissions) used since the Roman time for the famous thermal baths. The geothermal potential of the area has attracted the attention of national energy companies (SAFEN, ENEL, AGIP) that carried out some exploration campaigns between 1930 and 1980: 117 wells have been drilled in the area (26 in Campi Flegrei) reaching the maximum depth of 3046 m. The investigations have demonstrated that fluids with high temperatures are present at relative shallow depths in the area of Campi Flegrei and Ischia island. The industrial exploitation of the geothermal resources to produce electricity have never take off, because of the low cost of oil price in 80's, and the lack of interest for renewable energies (Carlino et al. 2012). Anyway the scientific researches on the area have continued with the aim of understand the geological settings, the hydrothermal system and the volcanic structures that lie under the surface of Campanian volcanoes. In December 2012, a new well has been drilled in Bagnoli plain within the Campi Flegrei Deep Drill Project in the framework of the International Continental Scientific Drilling Program (Carlino et al., 2016). The target of the project was the understanding of Campi Flegrei caldera dynamics and the study of geothermal reservoir.

Figure 2 - Campi Flegrei caldera (Carlino et al., 2012)

The dynamism of Campi Flegrei is characterized by the bradisism: uplift episodes of the ground and subsidence phases occurred over the centuries that have leaved clear traces. The seismicity of the area seems related to the uplift of the caldera (Carlino et al., 2010). The most seismically active period in the last 50 years, was between 1982 and 1984; during this period a lowering of the ground of about 1.8 meters occurred (Del Gaudio et al., 2010; Petrillo et al., 2013). The magnitude of the Phlegraean earthquakes is generally lower than 1.0, with a maximum magnitude of 4.0 in the period 1982-84 (De Natale, 1987). The majority of the events are located in the first 4 km and they are not detectable by the population but only by the instruments (Carlino et al., 2016).

A hot and saline geothermal system with by a geothermal gradient in the range 100÷170 °C/km is present in the subsoil of Campi Flegrei (Rosi and Sbrana, 1987; Barberi et al., 1991; Piochi et al., 2014; Mormone et al., 2015). According to Zollo et al. (2008) the conceptual model of the geothermal reservoir can be represented by a magmatic source located at the depth of 8-10 km, with a thickness of almost 1 km and a diameter equal to that of the caldera. The heat content is estimated to be about $6 \cdot 10^{12}$ Jm^{-2} per area. This primary source provides heat to the layers above. At a depth greater than 3-4 km, the fluids circulate very slow, therefore the heat is transferred due to conduction. In the shallower layers (0-2 km) an advective transport takes place, because of the high permeability due to the fracturing system which allows the fluids to flow to the surface. In any case, an accurate source modelling is out of the aims of this work; thus, we used a precautionary approach assuming the heat source as a purely conductive medium. Any advective contribution would results in better performances with respect to the one presented hereafter. The most interesting areas from the geothermal production point of view are Mofete, San Vito and Agnano, which are indicated in Figure 2. The Figure 3 shows the conceptual model of the Mofete geothermal reservoir, where three aquifers have been identified. The first aquifer is at the basis of the Neapolitan Yellow Tuff, between 500 and 1000 meters with 20% of vapour and temperatures in the range 100 ÷ 130 °C; the second aquifer is located within the zone of the calcium silicate and aluminum at a depth between 1800 and 2000 meters (40% of vapour and a average temperature of 300 °C); the deepest aquifer level is between 2500 and 2700 meters and it is probably a vapour dominated system (Carlino et al. 2012).

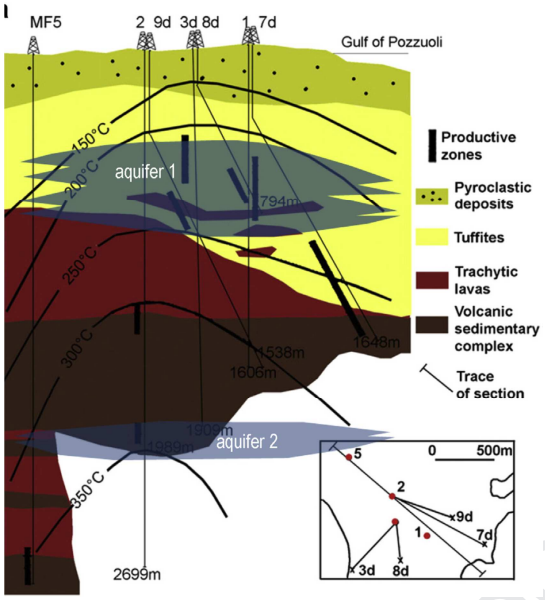

Figure 3 – Model of geothermal reservoir and acquifers (Carlino et al., 2016).

The deep borehole heat exchanger has been applied in the area of the wells Mofete 1 (MF1), Mofete 3d (MF3d) and Mofete 2 (MF2) drilled during the survey campaign of ENEL-SAFE (1977–1985). A representative stratigraphy of the area has been deduced from Carlino et al. (2012). The thermo-physical properties of the area are calculated using the average values weighted on the thickness of the layer (λ = 2.5 $Wm^{-1}K^{-1}$; ρ = 1900 $kg{\cdot}m^{-3}$; c_p = 1220 $Jkg^{-1}K^{-1}$). The average geothermal gradient is almost 150 °C/km (Figure 4).

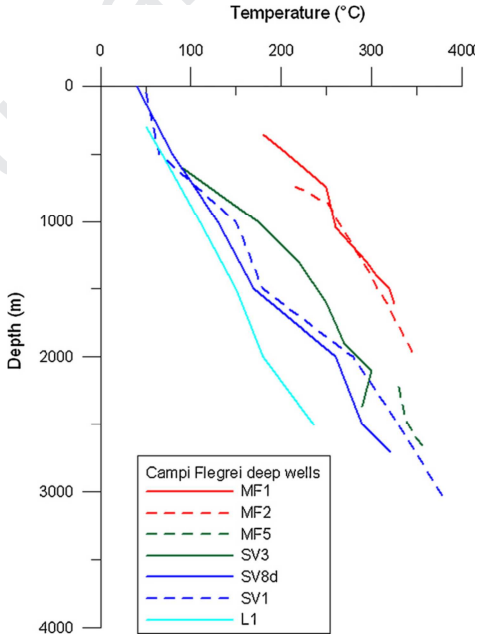

Figure 4 - Temperature profiles of Campi Flegrei deep wells (AGIP, 1987; Carlino et al. 2012).

A previous evaluation (Alimonti et al., 2016) about the area was carried out using a numerical model of the heat transfer phenomena in the WBHX based on the Fourier equation (for further details see Alimonti and Soldo, 2016). The results indicated that after 1 year of operation with the flow rate of 20 m^3/h, the outlet temperature of the fluid is about 150 °C, the thermal power is 2.5 MW and the electrical power is 250 kW. Regarding the electrical power production, the analysis has used either a model of ORC plant, or the relation of MIT (VV.AA 2006), which correlates the thermal efficiency of the

plant with the inlet temperature of the working fluid. Nevertheless, some components, like as the cooling tower and ancillary equipment, were neglected in the ORC model. In this paper, a comprehensive thermodynamic assessment of the WBHX+ORC plant has been carried out and all the thermodynamic parameters have been calculated, including the exergy and the exergy destruction. The target is to evaluate the energetic and exergy efficiency of the entire system and to identify the most inefficient components.

3. Energy and exergy analysis

In this section, we illustrate a comprehensive energy and exergy analysis of the reference WBHX - ORC system showed in Figure 5. Assumed working fluid is 2-methylpropane (isobutane) for the ORC power cycle, pure water as heat carrier fluid in the WBHX, and air as refrigerant fluid in the cooling tower. Thermo-physical properties are evaluated through the widespread software REFPROP (Lemmon et al., 2007). Components models, thermo-physical properties, energy and exergy balances are implemented in MS Excel spreadsheets and solved through the solver tool.

All the components of the ORC – WBHX systems are evaluated at the nominal working condition of the system, through zero-dimensional steady-state mass, energy, and exergy balances, together with the overall rate equation for the heat exchangers. The ground source is the only subsystem with a theoretical relevant dynamic behavior, but it can be assumed as stationary for the purposes of the present paper, as will be explained in Section 4. With reference to a generic WBHX – ORC power plant (see Fig. 5), the general energy balance of each component reads:

$$\dot{H}_{f,in} + \dot{Q} = \dot{H}_{f,out} + \dot{W} \quad [\mathrm{W}] \qquad (1)$$

where:

- $\dot{H}_f$ is the enthalpy of the fluid(s) entering/leaving the device, namely:
  $\dot{H}_f = \dot{m}_f h_f = \dot{m}_f (h_f - h_{f,0})$ (2)
- $\dot{Q}$ is the total thermal power(s) exchanged at the control surface of the device;
- $\dot{W}$ is the mechanical/electrical power transfer(s) at the control surface of the device (e.g. turbines, pumps, and fans).

The corresponding general exergy balance reads (Kotas, 1995):

$$\dot{E}x_{f,in} + \dot{E}x^{\dot{Q}} = \dot{E}x_{f,out} + \dot{E}x^{\dot{W}} + \dot{I} \quad [\mathrm{W}] \qquad (3)$$

where:

- $\dot{E}x_{f,}$ is the physical exergy of the fluid(s) entering/leaving the device, namely:

$$\dot{E}x_f = \dot{m}_f e x_f = \dot{m}_f \left[\left(h_f - h_{fa,}\right) - T_a \left(s_f - s_{fa,}\right) \right] \qquad (4)$$

- $\dot{E}x^{\dot{Q}}$ is the exergy associated with the thermal power exchange(s) at the control surface of the device, namely:

$$\dot{E}x^{\dot{Q}} = \int_A \dot{q} \left(\frac{T - T_a}{T}\right) dA \qquad (5)$$

- $\dot{E}x_{\dot{W}}$ is the exergy associated with a power transfer(s) at the control surface of the device. It exactly corresponds to the power transfer(s) $\dot{W}$.
- $\dot{I}$ is the exergy destruction associated with the irreversibly production rate.

The First-Law efficiency can be expressed by the ratio between the net work/power output and the inlet energy/power streams. In this work, we refer to the following expressions for direct or inverse energy conversion systems, respectively:

$$\eta^I = \frac{\dot{W}_{out} - \dot{W}_{in}}{\dot{H}_{f,in} - \dot{H}_{f,out}} \quad \text{or} \quad \eta^I = \frac{\dot{H}_{f,in} - \dot{H}_{f,out}}{\dot{W}_{in}} \qquad (6)$$

There are different expressions of the Second-Law (exergy) efficiency, η^{II}, presented in literature (Kotas 1995, Bejanet al. 1996, DiPippo 2012), e.g., rational efficiency, efficiency defect, functional exergy efficiency, exergy loss ratio. In this work, we refer to the exergy efficiency formulation proposed by Bejanet al. (1996), which is the ratio between the actual exergy output (product) and the required exergy input (fuel). η^{II} does not have a unique expression, but it depends on the specific component to be analyzed. With reference to the purposes of this work, we refer to heat exchangers, power turbines, and pumps. The following expressions apply:

$$\eta_T^{II} = \frac{\dot{W}_{out}}{\dot{E}x_{f,in} - \dot{E}x_{f,out}} \quad \eta_P^{II} = \frac{\dot{E}x_{f,in} - \dot{E}x_{f,out}}{\dot{W}_{in}} \quad \eta_{HX}^{II} = \frac{\dot{E}x_{f,out}}{\dot{E}x_{f,in}} \qquad (7)$$

These expressions are similar to the *task efficiency* proposed by Moran (1989). In other words, η^{II} provides a measure of the deviation between actual and maximum theoretical performance of the device (Casarosa et al., 2014). As discussed in Kotas (1995), cooling towers do not have a useful expression of η^{II}, as their primary function is to dissipate heat toward the environment. The typical performance index for this kind of systems is the ratio between the irreversibility rate, $\dot{I}$, and the heat exchanged, $\dot{Q}$, i.e., the efficiency defect. However, the latter definition is not comparable with the approach followed above to define η^{II}. In this work, we will evaluate cooling towers only in terms of energy consumption and irreversibility rate.

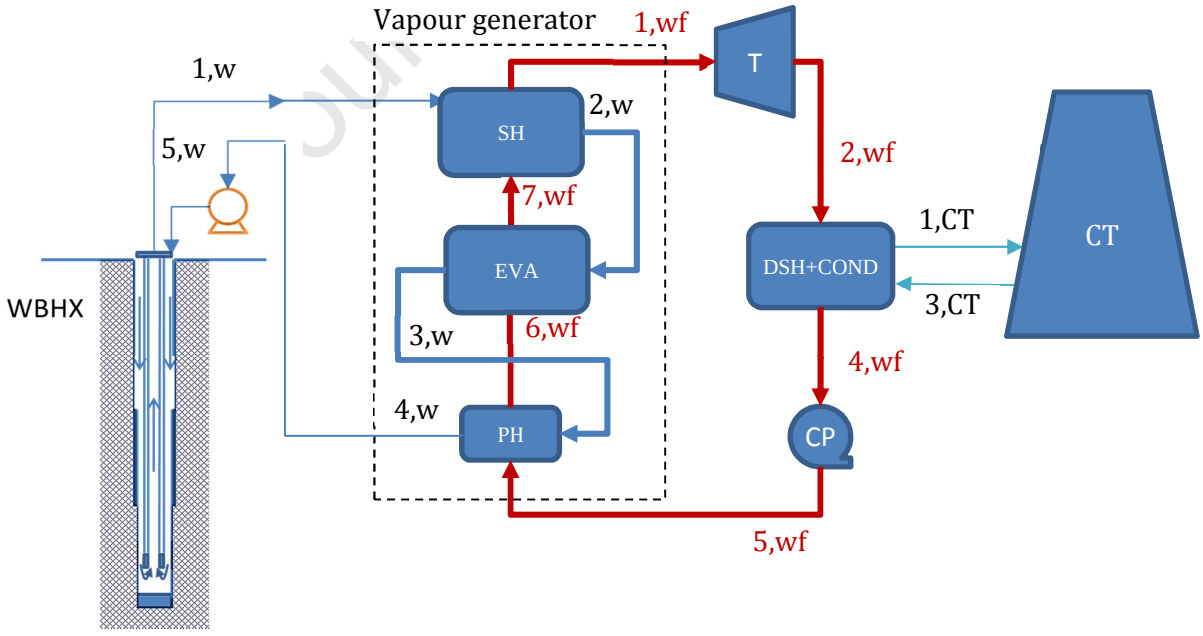

Figure 5 - Scheme of the analyzed WBHX – ORC system.

3.1 WBHX

This section includes both the coaxial well (Fig. 6) and the ground source (Fig. 7). The ground source is assumed as a purely conductive medium with the thermo-physical properties shown in Table 1.

According to Section 2, we assumed a constant thermal gradient of 15 K per meter of depth. The ground temperature profile goes from 50 °C at the surface to 350 °C at the bottomhole.

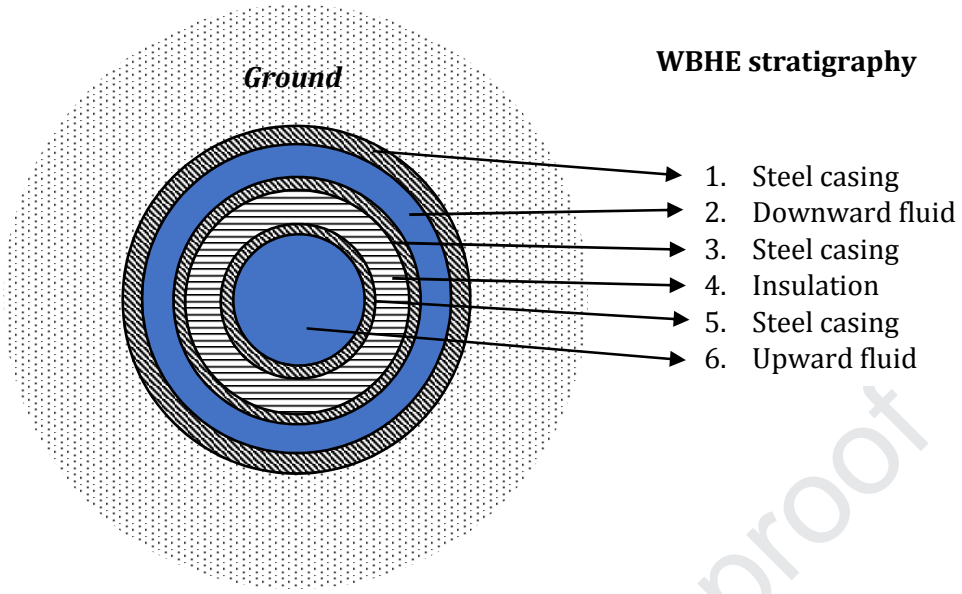

Figure 6 - WBHE axial section A-A.

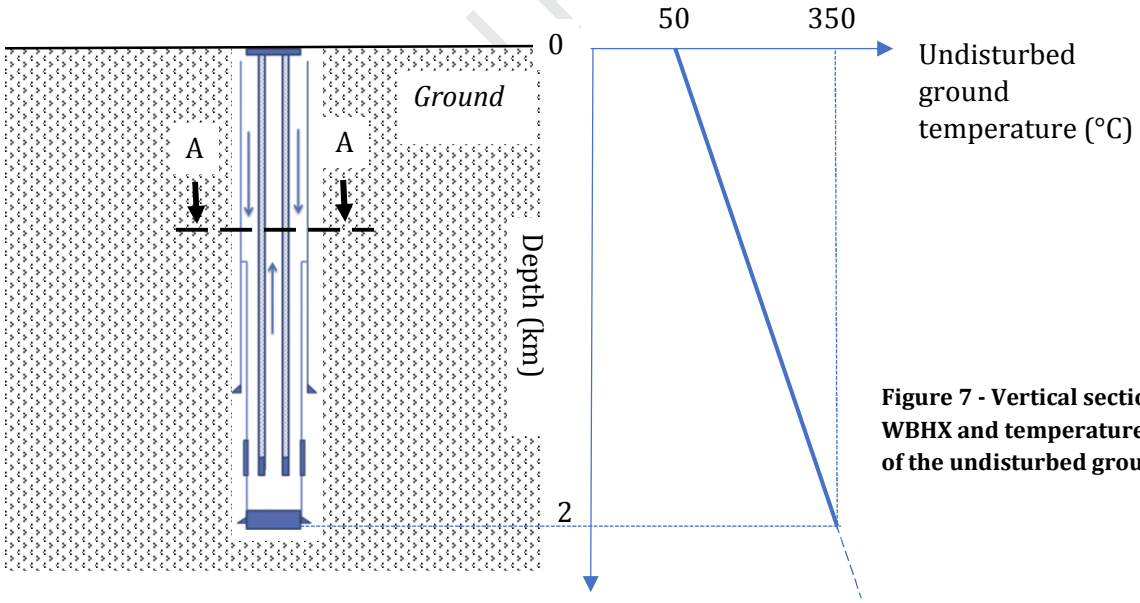

Figure 7 - Vertical section of the WBHX and temperature profile of the undisturbed ground.

Table 1 - Thermo-physical and geometrical parameters of the WBHX.

PARAMETER	VALUE	UNIT
Ground thermal diffusivity	1.08×10^{-6}	m^2/s
Thermal conductivity:		W/(m K)
- Ground	2.50	
- Steel	50.00	
- Concrete	1.30	
- Insulation material	0.04	
WBHX depth	2000	m

Inner/outer radius		
- *Layer 1*	0.150/0.178	m
- *Layer 2*	0.140/0.150	m
- *Layer 3*	0.121/0.140	m
- *Layer 4*	0.089/0.121	m
- *Layer 5*	0.078/0.089	m

The heat exchanged between the circulating fluid and the ground is evaluated through the set of thermal resistances shown in Figure 8.

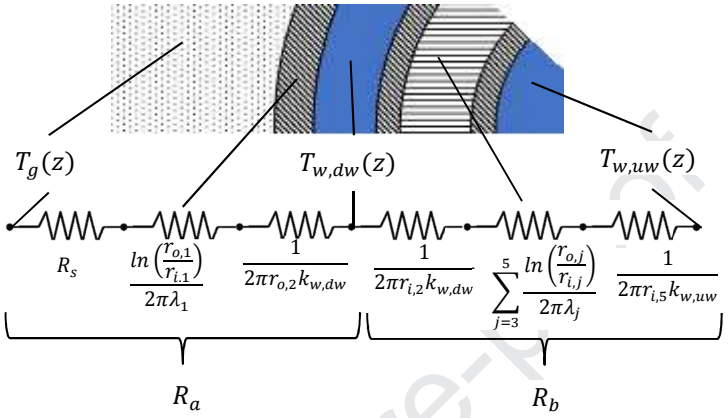

Figure 8 - WBHX thermal resistance model.

R_s is the transient thermal resistance between the external well casing surface and the undisturbed ground. Considering the assumption of a purely conductive medium and the slender geometry of the well, R_s value can be estimated through the classical line heat source theory (see, for instance, Conti 2016, Man *et al.* 2010). According to Alimonti and Soldo (2016), the radius of thermal influence due to the undergoing heat extraction can be evaluated as:

$$R_s = \frac{1}{2\pi\lambda_s}\ln\left(\frac{2\sqrt{\alpha_s t}}{r_{o,1}}\right) \qquad (8)$$

The conductive thermal resistance of the well strata is evaluated through the classical heat transfer theory for cylindrical geometries. $h_{w,dw}$ is the convection coefficient within the annulus. According to Lavine et al. (2001), for fully developed turbulent flow, the convection coefficient is approximately the same on the outer and inner surface. Both Nusselt and Reynolds numbers can be evaluated considering a hydraulic diameter of D_h. Finally, $h_{w,uw}$ is the convective coefficient in the upward pipe. In this work, we used the classical Dittus-Boelter equation to calculate all the convective coefficients (Lavine et al. 2001). With reference to Figure 8, we can thus define R_a as the thermal resistance between the downward fluid and the undisturbed ground temperature, R_b as the thermal resistance between the downward fluid and the upward fluid.

$$R_a = R_s + \frac{\ln\left(\frac{r_{o,1}}{r_{i,1}}\right)}{2\pi\lambda_1} + \frac{1}{2\pi r_{o,2}k_{w,dw}} \qquad (9)$$

$$R_b = \frac{1}{2\pi r_{i,2}k_{w,dw}} + \sum_{j=3}^{5}\frac{\ln\left(\frac{r_{o,j}}{r_{i,j}}\right)}{2\pi\lambda_j} + \frac{1}{2\pi r_{i,5}k_{w,uw}} \qquad (10)$$

The energy balance of the WBHX reads:

$$\dot{Q}_{WBHX} = \dot{m}_w c_w \left(T_{1,w} - T_{5,w}\right) \qquad (11)$$

where $\dot{Q}_{WBHX}$ is the total heat exchanged by the fluid with the ground. The outlet temperature $T_{5,w}$ and the temperature profile of the fluid along the WBHX is evaluated through the following set of equations:

$$\begin{cases} \dot{m}_w c_w \frac{dT_{w,dw}}{dz}(z) = \frac{T_s(z) - T_{w,dw}(z)}{R_a} - \frac{T_{w,dw}(z) - T_{w,uw}(z)}{R_b} \\ -\dot{m}_w c_w \frac{dT_{w,uw}}{dz}(z) = \frac{T_{w,dw}(z) - T_{w,uw}(z)}{R_b} \end{cases} \qquad (12)$$

with the following boundary conditions:

$$T_{w,dw}(0) = T_{1,w} \qquad T_{w,dw}(L) = T_{w,up}(L) \qquad (13)$$

The set of differential equation 12 is solved numerically to find the outlet temperature $T_{5,w} = T_{w,uw}(0)$ as a function of the mass flow rate, $\dot{m}_w$, and inlet temperature $T_{1,w}$.

The exergy balance of the WBHX is evaluated from the undisturbed ground to the circulating fluid, namely:

$$\dot{I}_{WBHX} = \dot{m}_w \left(ex_{5w} - ex_{1,w}\right) + \dot{E}x^{Q}_{WBHX} \qquad (14)$$

where:

$$\dot{E}x^{Q}_{WBHX} = \int_0^L \frac{T_s(z) - T_{w,dw}(z)}{R_1} \left(1 - \frac{T_a}{T_s(z)}\right) dz \qquad (15)$$

In Eq. 15, the integral argument is considered null when $T_s(z) < T_{w,dw}(z)$ to consider as irreversibilities the heat losses towards the ground.

3.2 WBHX pump

The pumping process of liquid water can be assumed as isentropic with a negligible error. Additionally, we neglected the pressure drop within the vapour generator, thus, the prevalence of the WBHX pump corresponds to the pressure losses within the well. However, to account for any electrical-mechanical inefficiency of the pump device, we assumed a standard value of the overall efficiency equal to 0.6 (DiPippo, 2012). The energy balance of the pump reads:

$$\dot{W}_{WP} = \dot{m}_w (p_{5w} - p_{1w})/\rho_w \qquad (16)$$

$$\dot{W}_{WP,el} = \dot{W}_{WP}/\eta_{WP,em} \qquad (17)$$

The pressure drop between the inlet and the outlet sections of the WBHX is evaluated through the classical Darcy–Weisbach equation, namely:

$$p_{5w} - p_{1w} = \int_0^H \xi_{dw} \frac{1}{D_h} \rho_w \frac{u_{dw}^2}{2} dz + \int_0^H \xi_{uw} \frac{1}{2r_{i,5}} \rho_w \frac{u_{uw}^2}{2} dz \qquad (18)$$

where the friction factor ξ is evaluated through the classical Moody diagram for fully developed turbulent flow (Lavine et al. 2001). The exergy balance reads:

$$\dot{m}_w \left(ex_{4,w} - ex_{5,w}\right) + \dot{W}_{WP,el} = \dot{I}_{WP} \qquad (19)$$

3.3 Power plant (ORC cycle)

The ORC section includes six components: preheater, evaporator, superheater, power turbine, condenser and feeding pump: the thermodynamic cycle is shown in Figure 9.

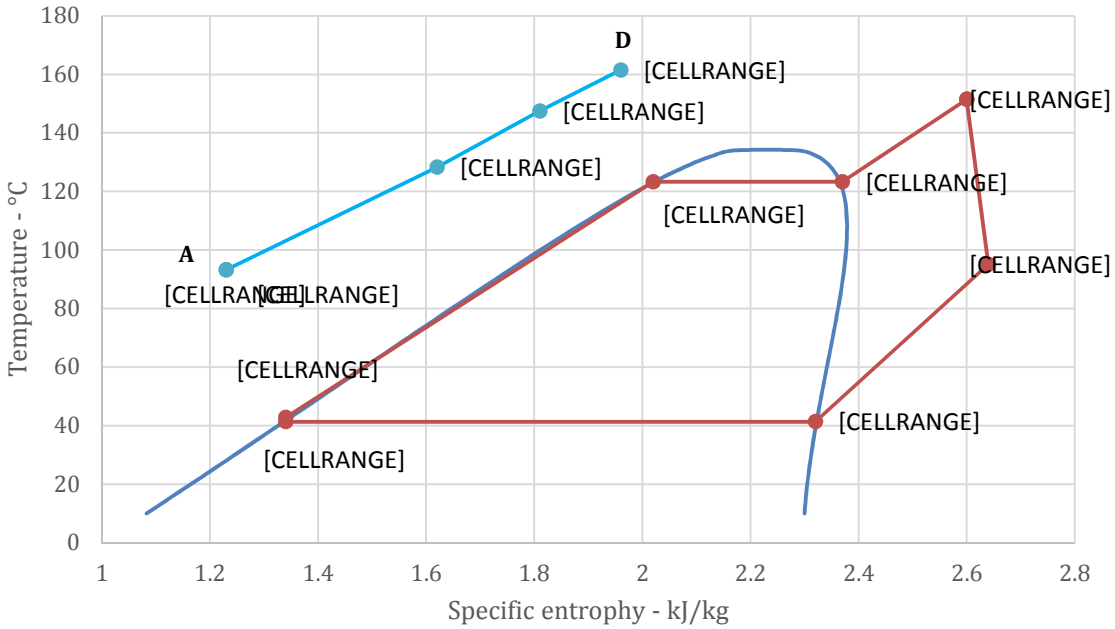

Figure 9 - TS diagram of the ORC

3.3.1 *Preheater, evaporator and superheater*

We evaluated the energy balance of all the three components of the steam generator. Both $\dot{W}$ and $\dot{Q}$ are assumed as negligible, leading to a conservation of the total enthalpy of the heating exchanging fluids. Working fluid flow rate, $\dot{m}_{wf}$, and inlet temperature to the power turbine, $T_{1,HC}$ are evaluated assuming a typical pinch point of 5 K (DiPippo, 2012) (see Fig. 10).

Since $\dot{W}$ and $\dot{Q}$ are assumed as null, the exergy destruction is evaluated as the difference between inlet and outlet fluid exergy, namely:

$$\dot{m}_w(ex_{3,w} - ex_{4,w}) + \dot{m}_{wf}(ex_{5,wf} - ex_{6,wf}) = \dot{I}_{PH} \qquad (20)$$

$$\dot{m}_w(ex_{2,w} - ex_{3,w}) + \dot{m}_{wf}(ex_{6,wf} - ex_{7,wf}) = \dot{I}_{EVA} \qquad (21)$$

$$\dot{m}_w(ex_{1,w} - ex_{2,w}) \mp \dot{m}_{wf}(ex_{7,wf} - ex_{1,wf}) = \dot{I}_{SH} \qquad (22)$$

3.3.2 Power Turbine

We assumed standard values of the isentropic efficiency and an electrical-mechanical efficiency 0.85 and 0.95, respectively (Zarrouk, 2014). The energy balance reads:

$$h_{2,wf} = h_{1,wf} - \eta_T(h_{1,wf} - h_{2is,wf}) \qquad (23)$$

$$\dot{W}_{T,el} = \dot{m}_{wf}(h_{1,wf} - h_{2,wf})\eta_{T,em} \qquad (24)$$

The exergy balance reads:

$$\dot{m}_{wf}(ex_{1,wf} - ex_{2,wf}) - \dot{W}_{T,el} = \dot{I}_T \qquad (25)$$

3.3.3 Circulation pump

The pumping process of a liquid fluid can be assumed as isentropic with a negligible error. However, as other external inefficiencies (i.e. friction or electromechanical losses) typical occurs in these devices, we considered an overall electric-mechanical efficiency of 0.6 (DiPippo, 2012). The energy balance reads:

$$h_{5,wf} - h_{4,wf} = \frac{(p_{5,wf} - p_{4,wf})}{\rho_{4,wf}} \quad (26)$$

$$\dot{W}_{CP,el} = \dot{m}_{wf} \frac{(p_{5,wf} - p_{4,wf})}{\rho_{4,wf}} \frac{1}{\eta_{P,em}} \quad (27)$$

The exergy balance reads:

$$\dot{m}_{wf}\left(ex_{4,wf} - ex_{5,wf}\right) + \dot{W}_{CP,el} = \dot{I}_{CP} \quad (28)$$

3.3.4 Desuperheater + Condenser device

In the desuperheater + condenser device, heat is transferred from the working fluid to the cooling system loop. As shown in Figure 10, we have a desuperheating section and a condensing one. The energy balance and the assumed a standard pinch point of 5 K (DiPippo, 2012) were used to evaluate the cooling loop flow rate, $\dot{m}_{CT}$, and the supply temperature to the cooling tower, $T_{1,CT}$.

$$\dot{m}_{wf}\left(h_{2,wf} - h_{4,wf}\right) = \dot{m}_{wCT}\left(h_{1,wCT} - h_{3,wCT}\right) \quad (29)$$

$$\dot{m}_{wf}\left(h_{2,wf} - h_{3,wf}\right) = \dot{m}_{wCT}\left(h_{1,wCT} - h_{2,wCT}\right) \quad (30)$$

$$T_{2,wCT} = T_{3,wf} - 5 \quad (31)$$

The inlet temperature, $T_{3,CT}$, of the cooling water is assumed equal to 25 °C (see Appendix A). The exergy balance reads:

$$\dot{m}_{wf}\left(ex_{2,wf} - ex_{4,wf}\right) + \dot{m}_{CT}\left(ex_{3,wCT} - ex_{1,wCT}\right) = \dot{I}_{DSH+COND} \quad (32)$$

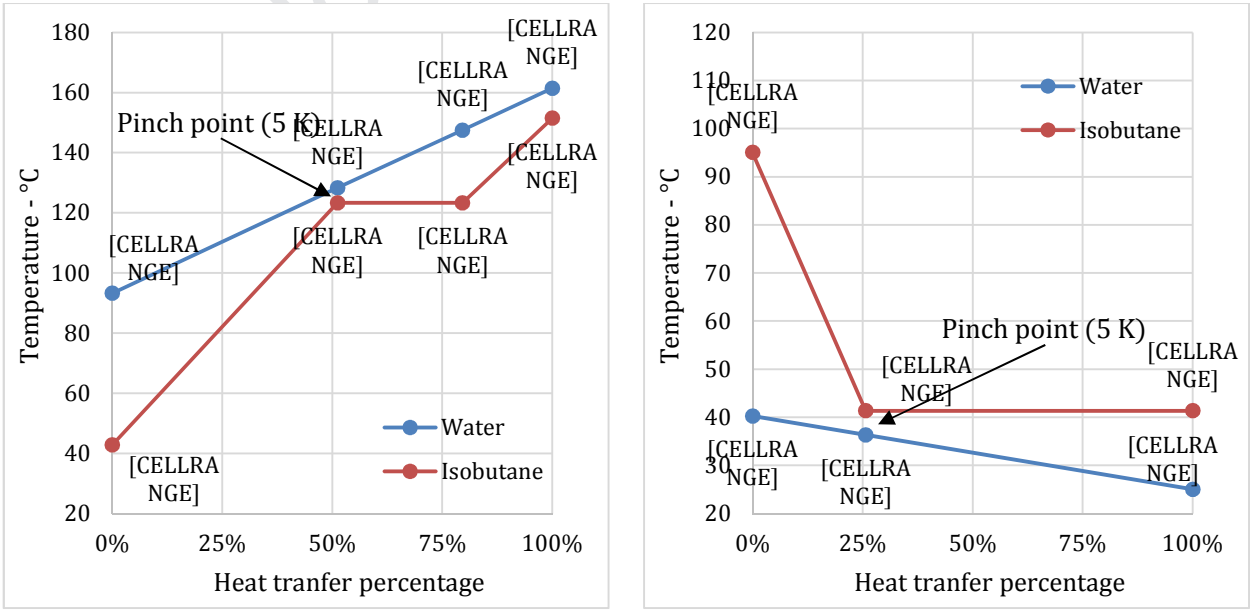

Figure 10 - Heat transfer vs temperature charts for the vapour generator (left) and desuperheater-condenser (right).

3.4 Cooling systems/towers

The cooling system was supposed to be a dry cooling tower, using compact fin-and-tube heat exchangers. As mentioned in (Franco and Villani 2009), cooling system represents a significant drawback for ORC viability, as its power consumption may reach up to 30% of turbine output. Therefore, we performed a specific analysis to minimize the impact of fans power consumption on the overall system. The sizing process of the heat exchanger is illustrated in Appendix A. Here, we just recall that we evaluated the required heat transfer surface through the classical logarithmic mean temperature difference method (LMTD). Then, we optimize the finned heat exchanger geometry, to minimize the fan power consumption at the given heat flow rate. The sizing results are shown in Table 6 and in Table A1.

Regarding exergy analysis, the inlet air is at the ambient condition without exergy content. We also assumed as dissipated the exergy of the outlet air stream; thus, the exergy balance reads:

$$\dot{m}_{wCT}\left(ex_{1,wCT} - ex_{3,wCT}\right) + \dot{W}_{CT,el} = \dot{I}_{CT} \qquad (33)$$

4. Results and discussion

In this work, we analyses the performance of the system shown in Figure 5 after one year of continuous operation. According to Alimonti and Soldo (2018), this period corresponds to the time required to obtain an increase rate of the ground thermal resistance, R_s, lower than 10%/yr. In other words, after one year, the ground source can be practically assumed as stationary and the estimated thermal radius is about 10 meters. Also the ground source can thus be modeled through a steady state approach as the rest of the system (see Section 3)

The overall system includes three main sections: the WBHX, the energy conversion system (ORC cycle), and the cooling system (cooling tower). The Table 3 shows the state points of the system (outputs) and the reference and ambient condition for each fluid. The assumed ambient state corresponds to the average annual outdoor air temperature and pressure in Italy, namely: $T_a = 20$ °C and $p_a = 0.1$ MPa. The condensing temperature is approximately 40 °C to ensure the operation of the cooling towers over the whole year. The Isobutane was found to be the operating fluid, after investigating the performance of Isobutane, Isopentane, R134a, R410a, and RC318 in terms of net power output. The WBHX flow rate, $\dot{m}_w$, and evaporation pressure, p_{EVA}, of the Isobutane have been selected through a sensitivity analysis on final system performances (see Table 2) in the range 4 – 8 m³/h and 20 – 30 bar, respectively. Table 2 shows that both efficiencies η^I and η^{II}, as well as power output $\dot{W}$, have a maximum at $p_{EVA} = 30\ bar$ and $\dot{m}_w = 6\ m^3/h$. Higher flow rates increase the power production, the efficiency of the ORC plant, but also the auxiliary energy consumption. The latter one leads to an overall reduction of system performances. As expectable, lower evaporation pressures decrease the efficiency of both ORC and overall system. Higher pressures are not considered to keep p_{EVA} at least 5 bar less than critical condition (36.5 bar).

Table 2 - Sensitivity analysis of the system as a function of the evaporation pressure and well flow rate.

$\dot{m}_w$	$4\ m^3/h$	$6\ m^3/h$	$8\ m^3/h$		$\dot{m}_w$	$4\ m^3/h$	$6\ m^3/h$	$8\ m^3/h$
$p_{EVA} = 30\ bar$								
η^I_{sys}	10.55%	**10.62%**	10.37%		η^I_{ORC}	11.64%	**11.67%**	11.63%
η^{II}_{sys}	23.28%	**23.15%**	22.11%		η^{II}_{ORC}	42.68%	**43.80%**	43.98%
$\dot{W}_{sys}$	45.15	**48.49**	47.64		$\dot{W}_{ORC}$	49.81	**53.29**	53.42

$p_{EVA} = 25\ bar$								
η_{sys}^{I}	9.63%	9.73%	9.65%		η_{ORC}^{I}	10.72%	10.82%	10.85%
η_{sys}^{II}	21.82%	21.55%	21.01%		η_{ORC}^{II}	39.95%	41.83%	42.67%
$\dot{W}_{sys}$	42.27	46.49	47.10		$\dot{W}_{ORC}$	47.05	51.70	52.95
$p_{EVA} = 20\ bar$								
η_{sys}^{I}	8.36%	8.53%	8.52%		η_{ORC}^{I}	9.44%	9.59%	9.66%
η_{sys}^{II}	19.18%	19.23%	18.99%		η_{ORC}^{II}	36.13%	38.64%	40.07%
$\dot{W}_{sys}$	38.11	43.11	44.67		$\dot{W}_{ORC}$	43.06	48.48	50.63

Table 3: Simulation results: state points of the WBHX – ORC system (outputs).

	T - °C	p - MPa	h – kJ/kg	s - kJ/(kg K)	ex* -kJ/K	$\dot{m}$ – kg/s
1,w	161.44	1.85	682.45	1.96	112.09	1.56
2,w	147.46	1.85	622.09	1.81	93.12	
3,w	128.29	1.85	540.17	1.62	69.63	
4,w	93.21	1.85	391.89	1.23	34.65	
5,w	93.22	2.00	392.05	1.23	34.81	
1,wf	151.44	3.00	783.56	2.60	158.55	0.96
2,wf	95.06	0.55	716.78	2.64	82.31	
3,wf	41.33	0.55	609.55	2.32	67.27	
4,wf	41.33	0.55	299.66	1.34	46.25	
5,wf	42.78	3.00	304.27	1.34	50.86	
6,wf	123.29	3.00	549.64	2.02	95.37	
7,wf	123.29	3.00	685.73	2.37	130.82	
1,wCT	40.25	0.3	170.48	0.58	2.91	6.24
2,wCT	36.33	0.3	152.45	0.52	2.03	
3,wCT	25.00	0.3	105.10	0.37	0.28	
Water ref. cond., $h_{w,0}$ $s_{w,0}$	0.01	6.12x 10^{-4}	0	0	3.93	
Working fluid ref. cond., $h_{wf,0}$ $s_{wf,0}$	0.00	0.157	200	1	-823.53	
Water amb. cond., $h_{w,a}$ $s_{w,a}$	20	0.1	84.01	0.30	0	
Working fluid amb. cond.,$h_{wf,a}$ $s_{wf,a}$	20	0.1	589.67	2.48	0	

* The exergy values refer to the ambient temperature and pressure.

Both energy and exergy balance of all subsystems and overall system are evaluated to calculate the net power output, irreversibilities, First-Law (energy) and Second-Law (exergy) efficiency. The resulting energy and exergy indexes of performance (outputs of the system) are shown in Table 4. The Table 5 summarize the operating parameters of the WBHX and the ORC (inputs of the system). The Table 6 reports the main cooling tower data (outputs). Figure 11 shows the temperature profiles of the WBHX.

Table 4: Simulation results: performance indexes (outputs) of the WBHX – ORC system.

Performance Index	Value
First-Law efficiency of the ORC	11.67%
First-Law efficiency of the overall system (including WBHX and cooling towers)	10.62%
Second-Law efficiency of the ORC	43.80%
Second-Law efficiency of the overall system (including WBHX and cooling towers)	23.15 %
WBHX capacity	453.19 kW_{th}

Net power output of the ORC, $\dot{W}_{ORC}$	53.29 kW_e
Net power output of the overall system, $\dot{W}_{sys}$	48.49 kW_e

Table 5 - Input and assumed operating parameters of WBHX and ORC.

PARAMETER	VALUE	UNIT
WBHX		
Circulating fluid	Water	
Flow rate, $\dot{m}_{f,w}$	6	m^3/h
Inlet pressure, $p_{5,w}$	2.0	MPa
R_s(after one year of operation)	0.31	mK/W
R_a	0.35	mK/W
R_b	1.90	mK/W
ORC Cycle		
Working fluid	2-methylpropane (Isobutane)	
Vapour Generator (Pre-heater, Evaporator, Super-heater)		
Pressure	3.0	MPa
Saturation temperature	123.29	°C
Pinch point	5	K
Power Turbine		
Isentropic efficiency, η_T	0.85	
Electro-mechanical efficacy, η_e	0.95	
Condenser		
Condensing pressure	0.55	MPa
Saturation temperature	41.33	°C
Pinch point	5	K
Circulation pump		
Electrical-mechanical efficiency, $\eta_{T,em}$	0.6	

Table 6 – Simulation results: m**ain cooling tower data outputs.**

Parameter	Value	Unit
Heat capacity	398.61	kW
Overall heat transfer coefficient, U_g	22.96	$W/(m^2K)$
Total heat transfer surface (air side)	$2.37x10^3$	m^2
Outlet water temperature, $T_{3,c}$	25	°C
NTU	2.09	
Heat transfer effectiveness, ϵ	0.75	
Overall finned surface efficiency, η_R	0.92	
Electrical fans power	4.39	kW

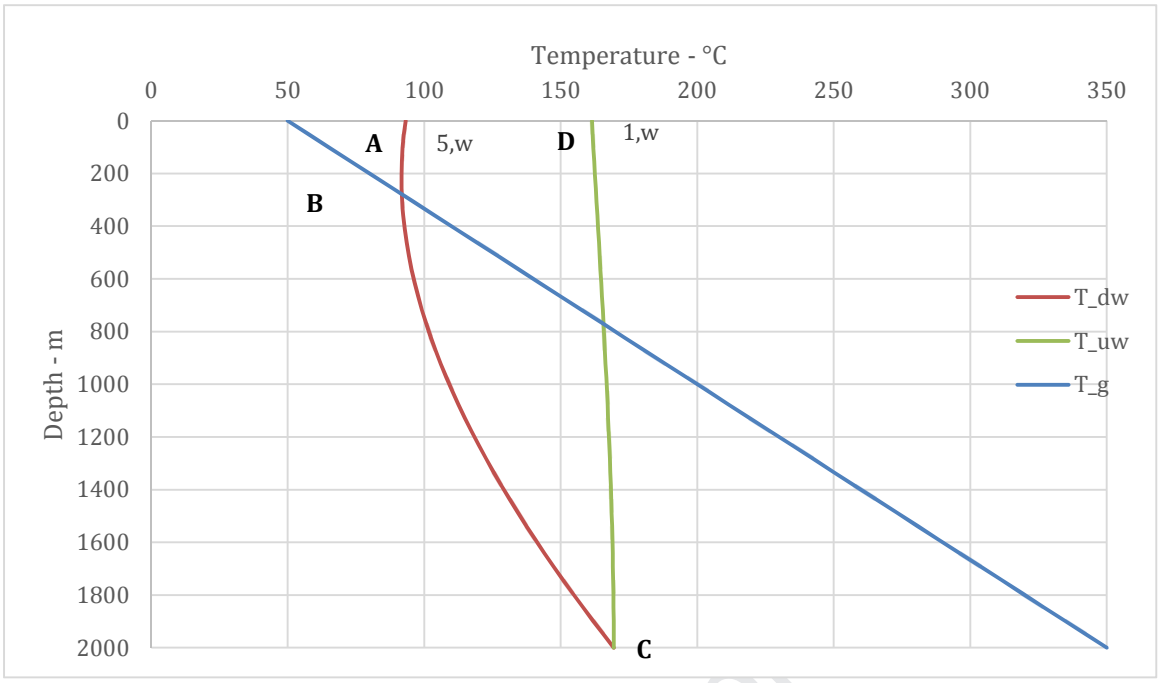

Figure 11- Temperature profiles along the WBHX.

The values in Table 4 indicate a good performance of the ORC cycle, with a First-Law efficiency of 11.67% and a Second-Law efficiency of about 43.80%. These values are similar to those of classical binary geothermal power plants, directly using geothermal brine (DiPippo 2012). The overall system performances decrease to 10.62% and 23.15% in terms of energy and exergy efficiency, respectively. The decrease of energy efficiency is mainly due to the fans energy requirements in the cooling tower. We recall that the fans energy consumption has been optimized through the procedure described in Appendix A, therefore, the energy loss due to the ancillary systems of WBHX – ORC plants might be higher.

The Figure 12-a and 12-b provides useful indications of the thermodynamic losses of the ORC plant. The Figure 12-a shows the irreversibility rate, $\dot{I}$, for the ORC components. The main exergy destruction occurs in the desuperheater – condenser (35%), followed by the power turbine and the pre-heater device (both 24%). In Figure 12-a we also highlighted the exergy destruction rate due to the electrical-mechanical efficiency of each component. Totally, they account for the 11.8% of the total exergy destruction (6.13 kW vs 52.01 kW). In terms of Second-Law efficiency (Fig. 12-b), the lower values occur for the power turbine (83%), the desuperheater – condenser (78%), and the circulation pump (60%). However, the inefficiencies of the latter device are only related to the electrical-mechanical components.

The desuperheater – condenser has the higher $\dot{I}$ value and a low exergy efficiency. This is due to the desuperheating section that increases the average of the temperature difference between the two heat exchanging fluids, dissipating the still significant exergy content of the isobutane at the turbine outlet. A possible improvement could consist of a regenerative heat exchanger between the desupereating and the preheating section, downstream the turbine. This solution will increase the complexity of the plant and its viability will be analyzed in future work, by assessing the actual increment of the system exergy efficiency

The preheater has a significant $\dot{I}$ value, but its Second-law efficiency is higher than 90%. It is thus hard to figure out viable development solutions of this device, but the already mentioned regenerative heat exchanger.

The pump and turbine irreversibility production are related to the component technology (i.e., η_T, $\eta_{T,em}$, and $\eta_{P,em}$). An increased electro-mechanical efficiency would increase the ORC second-Law efficiency up to 49.0%. A higher increment is expected increasing η_T value, as it results for the 17.4% of current irreversibilities.

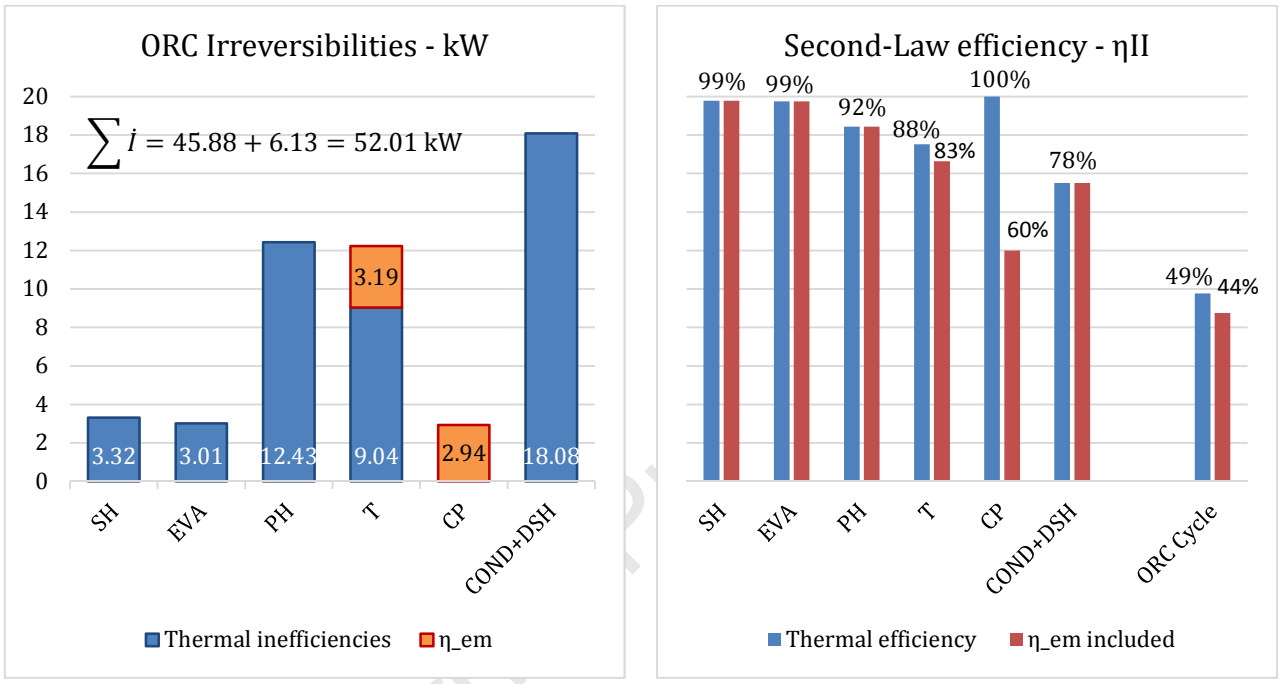

Figure 12 – Irreversibilities (a) and Second-Law efficiency (b) values for each ORC component

Regarding the overall system, we note that the overall First-Law and Second-Law efficiencies reduce to 10.62% (-9.01%) and 23.15% (-47.15%), respectively (Table 4). The energy losses are mainly due to the electricity requirement of the cooling tower (fans), which requires about 4 kW of electrical energy (7.2% of the turbine output). The well pump requires about 0.4 kW, which corresponds to the 0.7% of the turbine output. Shortly, the ancillary subsystems accounts for the 7.9% of the gross output of the ORC turbine.

In terms of exergy destruction, we note that the overall Second-Law efficiency is practically halved with respect to the sole ORC cycle. This reduced value is mainly due to the large exergy destruction occurring in the WBHX (see Fig. 13-a), which suffers from the main irreversibility rate (88.05 kW). Figure 13-b confirms this interpretation: even if we improved the electrical-mechanical efficiency of the well pump, we would not achieve significant increases of the exergy efficiency. The exergy destruction occurring in the cooling tower is mainly due to heat to be released in the ambient by the ORC cycle: it represents an intrinsic thermal loss of the energy conversion cycle and depends on ORC condensing temperature and heat transfer effectiveness of the cooling apparatus. In this work, the latter equipment has been optimized to reduce the fans power (see in Fig. 13-a the reduced $\dot{I}$ due to the fans electricity consumption), however different results might be obtained if one set $\dot{I}_{CT}$ as objective function. The Table 7 reports the terms used to calculate the irreversibilities for each components. As mentioned in Section 3, Figure 13–b does not show the η^{II} value of CT, as is it not

possible to derive a comparable expression among dissipative devices and the other system components (Kotas, 1995).

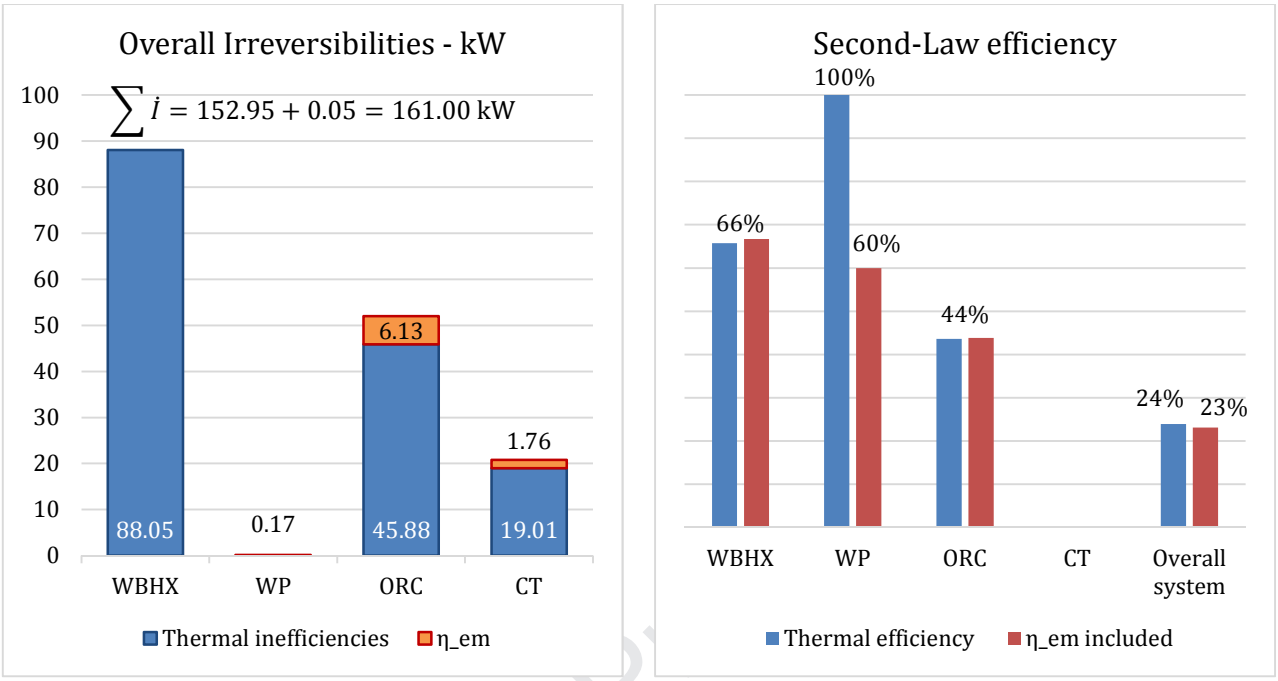

Figure 13 – Irreversibilities (a) and Second-Law efficiency (b) values for the main components of the overall system

Table 7 – Terms of the exergy balance for each component

		WBHX	***WP***	***SH***	***EVA***	***PH***	***T***	***CP***	***COND+DSH***	***CT***
$\dot{E}_{in}$	kW	54.69	54.44	301.14	237.44	158.01	151.51	44.20	80.43	18.15
$\dot{E}_{out}$	kW	176.12	54.69	297.82	234.42	145.58	82.31	48.60	62.35	1.77
$\dot{E}^{Q}$	kW	209.48								
$\dot{W}_{el}$	kW		0.41				60.63	7.34		4.39
$\dot{I}$	kW	88.05	0.17	3.32	3.01	12.43	12.23	2.94	18.08	20.77

The main exergy destruction occurs in the WBHX, thus we deeply analyzed this component to find out causes and possible improvement actions.

We separately analyzed the downward duct (i.e., the annulus) and the upward one. (i.e., the central pipe). Besides, following the classical exergy theory, we divided the total exergy in its physical, kinetic, and potential components. The irreversibility production related to each phenomenon occurring in the WBHX is evaluated through the *restoring work* concept (Kotas, 1995). For instance, the irreversibility production rate associated to the friction losses in a fluid stream corresponds to the minimum work required to restore the original fluid pressure using an ideal reversible compressor. Additional details on restoring work and irreversibility production of typical energy processes are presented in Kotas (1995).

The first part of the downward duct (A - B in Fig. 11) is characterized by a heat loss through the ground. The exergy losses are due to the fluid temperature decrease, friction losses and to the short-circuit heat transfer from the upward duct. The second part of the downward duct (B – C in Fig. 11) is characterized by the heat transfer from the ground to the circulating fluid. The exergy losses are due to

the friction losses and to the heat exchange with the ground source and the upward duct. Finally, the upward duct (C – D in Fig. 11) is characterized by the thermal loss through the downward anulus. Here, the exergy losses are due to the temperature reduction and friction losses. Table 8 and Figure 14 show the value of each irreversibility production rate.

Table 8 - Exergy losses / restoring power (kW) associated to each phenomena occurring in the WBHX.

Phenomenon	Downward section		Upward section
	A - B	B -C	C -D
Temperature difference between the inlet and the outlet sections	-2.03	139.72	-16.03
Pressure difference between the inlet and the outlet sections	3.78	25.16	-29.18
Gravity work	-3.95	-26.87	30.83
Heat transfer between the upward and downward duct	-3.69	-13.97	
Heat transfer between the ground and the downward duct		-209.48	
TOTAL	**-5.89**	**-85.44**	**-14.38**

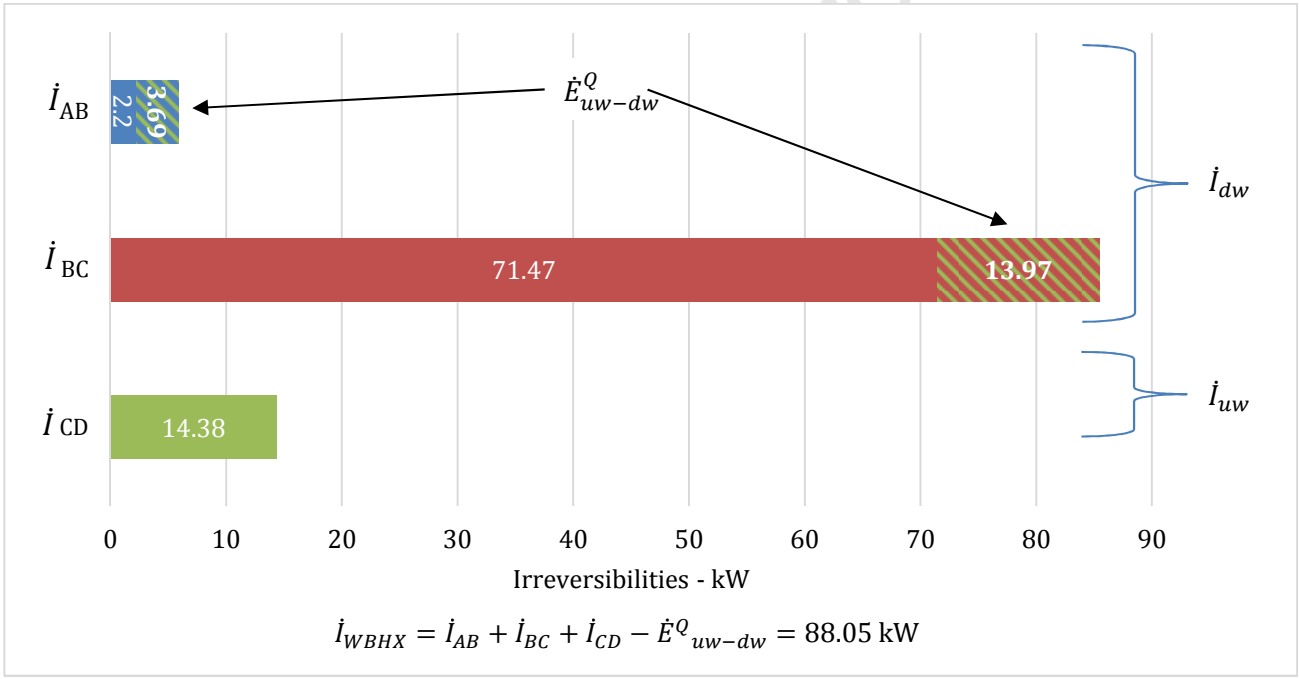

Figure 14 - Irreversibility production rates within the WBHX. The dashed areas correspond to the exergy losses due to the shorth-circuit heat transfer between the upward and downward ducts.

According to Table 8 and Figure 14, the main exergy loss depends on the heat exchange between the downward duct and the undisturbed ground ,in the B – C section, $\dot{Q}_{g,BC}$, followed by the shorth-circuit heat transfer between the upward and downward ducts. As third one, we have the heat loss toward the ground in the first part of the well (A – B). Finally, we have friction losses.

The heat losses toward the ground represent a lower exergy destruction with respect to the other two as the fluid and the ground have close temperatures that reduce the heat transfer and the exergy destruction. As reasonably expected, the shorth-circuit represent a notable contribution to the overall irreversibility production in the WBHX: $\dot{I}_{uw}$ is mainly related to the insulation performance between the two ducts and therefore can be reduced by increasing the thermal resistance R_2.

The first irreversibility production depends on the temperature deviation between the ground and the fluid and refers to the thermal resistance R_1: the higher the thermal resistance, the higher the exergy loss. At the typical operation periods of a power plant (i.e. years), R_s is the main contribution of R_1. Considering that R_s is inversely proportional to the thermal conductivity of the rock, one possible solution to improve the WBHX performance consists of fracturing the rock and the use of high conductivity material to fill the fractures, as proposed by (Taleghani et al., 2015). Nevertheless, the authors advise against the use of fracturing techniques in the area of Campi Flegrei, characterized by a very high urbanization, where the social response to soil stimulation methods will be probably negative. This means that enhancement techniques of the geothermal reservoir are poorly employable in the area. A more suitable solution consists of reducing the equivalent thermal radius of the well, namely the ground region affected by the heat transfer. Under equal operating conditions, a possible improvement strategy would consist of different heat extraction profiles through the control of the flow rate over the plant lifetime. A reduced thermal radius would lead to a more sustainable and efficient operation of the WBHX and higher η^{II} of the overall system.

5. Conclusions

A comprehensive thermodynamic analysis of a possible WBHX - ORC power plant located in the geothermal area of Campi Flegrei (Italy) has been presented. With respect to previous works on the same subject, the evaluation has accounted for all system components (i.e., the ground source, the WBHX, the ORC cycle, and the cooling system) to assess the potential of the technology in the area, also evaluating the impact of the ancillary systems and geothermal source response to the system performance. The state points of all subsystems have been calculated, as well as the energy and exergy performance indexes of each subsystems and the overall net power, First-Law efficiency, Second-law efficiency, and irreversibilities. The cooling tower design, the ORC operational flow rates and pressures have been optimized in order to maximize the net power output of the system, reducing the ancillary energy demand.

The results indicate that the source and the cooling system are predominant with respect to the power cycle. The ORC performance is actually similar to those of classical binary geothermal power plants, with a First-Law efficiency of 11.67% and a Second-Law efficiency of about 43.80%, The main exergy destruction occurs in the desuperheater – condenser as its saturation pressure cannot be lowered below a given value as the corresponding saturation temperature must be high enough to ensure the heat exchange with the cooling apparatus. Similarly, the neglection of the actual thermal response of the geothermal source leads to an overestimation of the thermal power entering the system, power output and efficiency. A regenerative heat exchanger between the desupereating and the preheating section, downstream the turbine, shall be evaluated to improve the performance of the ORC. Regarding the preheater, the pump and the turbine, the irreversibilities are related to the technological limits of the components (i.e., pinch point and electrical-mechanical efficiencies).

The overall system performances decrease to 10.62% due to the fans energy requirements in the cooling tower. The Second-Law efficiency is 23.15%, almost the half of the exergy efficiency of the sole ORC cycle. This reduction is mainly due to the large exergy destruction occurring in the WBHX, which suffers from the main irreversibility rate; therefore, a deep analysis of the component has been carried out. The WBHX has been studied considering separately the downward duct and the upward duct, calculating in each section the exergy losses associated to all thermal and fluid dynamic phenomena. The downward pipe has been divided in two parts: the first part characterized by exergy losses towards the shallow part of the ground and consequential fluid temperature decrease, by the friction losses, and to the short-circuit heat transfer with the upward duct; the second part is characterized by the exergy losses due to the heat exchange between the ground source and the upward duct, by the

abovementioned short-circuit heat transfer, and by the friction losses. The upward duct is characterized by the temperature decrease due to the thermal loss through the downward annulus and friction losses.

The results have shown that the overall irreversibility is strongly affected by the insulation performance between the two ducts and by the temperature deviation between the ground and the fluid. In order to obtain higher performance of the WBHX, possible strategies refer to both increasing the thermal resistance of the material insulating the two ducts of the WBHX annulus, the use of nanoparticles to increase the thermo-physical properties of the heat carrier fluid and new design in which two-phase flow and natural convection take place (i.e. geothermal convector), and the reduction of the equivalent thermal radius of the well. As already discussed, the latter solution is expected to be the more effective one, as even in case of a perfect insulation of the internal pipe, the temperature profiles along the WBHX indicate a limited increase of the outlet temperature. Similarly, even in case of an ideal heat transfer performance of the well (i.e, $R_a = R_s$), the equivalent thermal resistance of the geothermal source would result in a very similar irreversibility production. The employment of different and optimized heat extraction strategies, under equal ground source and ambient conditions, may lead to a more sustainable and efficient operation of the overall WBHX – ORC system with higher $\eta^{II}$and power output. The increase of the thermal conductivity of the ground by fracturing the soil surrounding the external casing and filling the fractures with a high conductivity material could be an improvement strategy of the WBHX, but not feasible for the site of Campi Flegrei.

In this regard, a precautionary pure conductive model has been adopted in the present work. Nevertheless, the geological and hydrological structure of Campi Flegrei produces an advective transport in the first 2 kilometers, which is expected to produce a recovery action with respect to the heat extracted from the ground, thus increasing the sustainability in time of the WBHX. A comprehensive study, including both reservoir modeling and power plant is advisable to evaluate this phenomenon and the effects on the overall system performance.

References

AGIP. Geologia e geofisica del sistema geotermico dei Campi Flegrei, Technical report. Settore Esplor e Ric Geoterm-Metodol per l'Esplor Geotermica, San Donato Milanese Italy 1987;1–23.

Akhmadullin I, Tyagi M: Design and analysis of electric power production unit for low enthalpy geothermal reservoir applications. World Academy of Science, Engineering and Technology, International Journal of Environmental, Chemical, Ecological, Geological and Geophysical Engineering, Vol: 8, No: 6, 2014.

Alimonti C, Soldo E: Study of geothermal power generation from a very deep oil well with a wellbore heat exchanger. Renewable Energy 2016, 86: 292-301.

Alimonti C, Soldo E, Berardi D, Bocchetti D: A comparison between energy conversion systems for a power plant in Campi Flegrei geothermal district based on a WellBore Heat eXchanger. Proceedings of European Geothermal Congress 2016 – Strasbourg (France) – 19-23 September 2016.

Ahmadi GR, Toghraie D: Energy and exergy analysis of Montazeri Steam Power Plant in Iran. Renewable and Sustainable Energy Reviews 56 (2016) 454–463.

Baba A, Ozgener L, Hepbasli A: Environmental and Exergetic Aspects of Geothermal Energy. Energy Sources, Part A, 28:597–609, 2006.

Barbacki A: Classification of geothermal resources in Poland by exergy analysis—Comparative study. Renewable and Sustainable Energy Reviews 16 (2012) 123– 128.

Barberi F, Cassano E, La Torre P, Sbrana A, (1991). Structural evolution of Campi Flegrei caldera in light of volcanological and geophysical data. J. Volcanol. Geotherm. Res. 48, 33–49.

Bejan A, Tsatsaronis G, Moran M: Thermal Design and Optimization. Wiley, New York, 1996.

Bertani R: Geothermal power generation in the world 2010–2014 update report. Geothermics 2016, 60, 31–43.

Bodvarsson G, Eggers DE. The exergy of thermal waters. Geothermics 1972;1:93–5.

Branislav MJ, Srbislav BG, Boris RL (2006). Research on the air pressure drop in plate finned tube heat exchangers. International Journal of Refrigeration 29(7), 1138-1143.

Bu X, Ma W, Li H: Geothermal energy production utilizing abandoned oil and gas wells. Renewable Energy 2012, 41: 80-85.

Carlino S, Somma R (2010). Eruptive versus Non-eruptive Behaviour of Large Calderas: the Example of Campi Flegrei Caldera (Southern Italy), Bulletin of Volcanology, 2010.

Carlino S, Somma R, Troise C, De Natale G: The geothermal exploration of Campanian volcanoes: Historical review and future development. Renewable and Sustainable Energy Reviews 16, (2012), 1004– 1030.

Casarosa C, Conti P, Franco A, Grassi W, Testi D: Analysis of thermodynamic losses in ground source heat pumps and their influence on overall system performance. Journal of Physics: Conference Series 2014, 547: p# 012006.

Cei M, Bertani R, Fiorentini A, Romagnoli P: Evaluation of heat exchange in a geothermal well. Proceedings of European Geothermal Congress 2013, Pisa, Italy 3-7 June 2013.

Cheng WL, Li TT, Nian YL, Wang CL: Studies on geothermal power generation using abandoned oil wells. Energy 2013, 59: 248-254.

Conti P: Dimensionless Maps for the Validity of Analytical Ground Heat Transfer Models for GSHP Applications. Energies 2016, 9, p# 890.

Coskun C, Oktay Z, Dincer I: New energy and exergy parameters for geothermal district heating systems. Applied Thermal Engineering 29 (2009) 2235–2242.

Davis AP, Michaelides EE: Geothermal power production from abandoned oil wells. Energy 2009, 34: 866-872.

De Natale G, Iannaccone G, Martini M, Zollo A, (1987). Seismic Sources and Attenuation Properties at the Campi Flegrei Volcanic Area, vol. 125, 1987, pp.883-917, 6.

Del Gaudio C , Aquino I, Ricciardi GP, Ricco C, Scandone R, (2010). Unrest episodes at Campi Flegrei: a reconstruction of vertical ground movements during 1905–2009. J. Volcanol. Geotherm. Res. 195, 48–56. http://dx.doi.org/10.1016/j.jvolgeores.2010.05.014.

DiPippo R, (2004). Second law assessment of binary generating power from low-temperature geothermal fluids. Geothermics 33, 565–586.

DiPippo R, Geothermal Power Plants, 3rd edition, Butterworth-Heinemann, 2012.

DiPippo R: Geothermal power plants: Evolution and performance assessments. Geothermics 2015, 53, 291–307.

Etemoglu AB, Can M: Classification of geothermal resources in Turkey by exergy analysis. Renewable and Sustainable Energy Reviews 11 (2007) 1596–1606.

Fallah M, Akbarpour Ghiasi R, Hasani Mokarram N: A comprehensive comparison among different types of geothermal plants from exergy and thermoeconomic points of view. Thermal Science and Engineering Progress 5 (2018) 15–24.

Feng Y, Tyagi M, White CD: A downhole heat exchanger for horizontal wells in low-enthalpy geopressured geothermal brine reservoirs. Geothermics 2015, 53: 368-378.

Franco A., Villani M. (2009). Optimal design of binary cycle power plants for water-dominated, medium-temperature geothermal fields. Geothermics, 38(4), 379–391.

Frass F, Hofmann R, Ponweiser K. Principles of finned-tube heat exchanger design for enhanced heat transfer. WSEAS Press, 2nd ed (2015), ISBN: 978-960-474-389-6.

Galoppi G, Biliotti D, Ferrara G, Carnevale EA, Ferrari L: Feasibility study of a geothermal power plant witha double-pipe heat exchanger. Energy Procedia 2015, 81: 193-204.

Ganjehsarabi H, Gungor A, Dincer I: Exergetic performance analysis of Dora II geothermal power plant in Turkey. Energy 46 (2012) 101-108.

Gökgedik H, Yürüsoy M, Keçebas A: Improvement potential of a real geothermal power plant using advanced exergy analysis. Energy 112 (2016) 254-263.

Hong KT and Webb R. (1996). Calculation of Fin Efficiency for Wet and Dry Fins. HVAC&R Research, 2(1), 27–41.

Jalilinasrabadya S, Itoi R, Valdimarssonb P, Saevarsdottirc G, Fujii H: Flash cycle optimization of Sabalan geothermal power plant employing exergy concept. Geothermics 43 (2012) 75–82.

Jalilinasrabady S and Itoi R: Classification of Geothermal Energy Resources in Japan Applying Exergy Concept. International Journal Of Energy Research 2013; 37:1842–1850.

Kestin J. Available work in geothermal energy. In: Kestin J, editor. Source book on the production of electricity from geothermal energy. Washington: US Government Printing Office; 1980. p. 227–75.

Kohl T, Brenni R, Eugster W: System performance of a deep borehole heat exchanger. Geothermics 2002, 31: 687-708.

Koroneos C, Polyzakis A, Xydis G, Stylos N, Nanaki E: Exergy analysis for a proposed binary geothermal power plant in Nisyros Island, Greece. Geothermics 70 (2017) 38–46.

Kotas TJ: The exergy method of thermal plant analysis. Krieger Publishing Company, Malabar (FL), 1995.

Kujawa T, Nowak W, Stachel AA: Utilization of existing deep geological wells for acquisitions of geothermal energy. Energy 2006, 31: 650-664.

Lavine AS, DeWitt, DP, Bergman TL, Incropera FP,. (2011). Fundamentals of Heat and Mass Transfer (7th ed.). Hoboken (NJ): John Wiley & Sons, Inc

Le Lous M, Larroque F, Dupuy A, Moignard A: Thermal performance of a deep borehole heat exchanger: Insights from a synthetic coupled heat and flow model. Geothermics 2015, 57: 157–172.

Lee KC: Classification of geothermal resources by exergy. Geothermics 30 (2001), 431-442.

Lemmon EW, Huber ML, McLinden MO: NIST Reference Fluid Thermodynamic and Transport Properties - REFPROP. Version 8.0 User's Guide. Physical and Chemical Properties Division National Institute of Standards and Technology Boulder, Colorado 80305, April 2007

Man Y, Yang H, Diao N, Liu J, Fang Z: A new model and analytical solutions for borehole and pile ground heat exchangers. Int. J. Heat Mass Transf. 2010, 53, 2593–2601.

Mokhtari H, Hadiannasab H, Mostafavi M, Ahmadibeni A: Determination of optimum geothermal Rankine cycle parameters utilizing coaxial heat exchanger. Energy 2016, 102: 260-275.

Moran MJ: Availability analysis: a guide to efficient energy use – Corr. Ed. New York: ASME Press, (1989).

Mormone A, Troise C, Piochi M, Balassone G, Joachimski M, De Natale G, (2015). Mineralogical, geochemical and isotopic features of tuffs from the CFDDP drill hole: Hydrothermal activity in the eastern side of the Campi Flegrei volcano (southern Italy). Journal of Volcanology and Geothermal Research 290 (2015) 39–52.

Nalla G, Shook GM, Mines GL, Bloomfield KK: Parametric sensitivity study of operating and design variables in wellbore heat exchangers. Geothermics 2005, 34: 330–346.

Noorollahi Y, Pourarshad M, Jalilinasrabady S, Yousefi H: Numerical simulation of power production from abandoned oil wells in Ahwaz oil field in southern Iran. Geothermics 2015, 55: 16-23.

Ozgener L, Hepbasli A, Dincer I, (2004). Thermo-mechanical exergy analysis of Balcova geothermal district heating system in Izmir, Turkey. ASME J. Energy Resour. Technol. 126, 293–301.

Ozgener L, Hepbasli A, Dincer I: Energy and exergy analysis of the Gonen geothermal district heating system, Turkey. Geothermics 34 (2005) 632–645.

Petrillo Z, Chiodini G, Mangiacapra A, Caliro S, Capuano P, Russo G, Cardellini C, Avino R, (2013). Defining a 3D physical model for the hydrothermal circulation at Campi Flegrei caldera (Italy). Journal of Volcanology and Geothermal Research 264 (2013) 172–182.

Piochi M, Kilburn C, Di Vito MA, Mormone A, Tramelli A, Troise C, De Natale G, (2014). The volcanic and geothermally active Campi Flegrei caldera: an integratedmultidisciplinary image of its buried structure. Int. J. Earth Sci. 103, 401–421.

Quijano J: Exergy analysis for the Ahuachapan and Berlin geothermal fields, El Salvador. Proceedings World Geothermal Congress 2000, Kyushu - Tohoku, Japan, May 28 - June 10, 2000.

Ramajo H, Tritlla J, Levresse G, Tello-Hinojosa E, Ramírez G, and Pérez H: New SExI tools to evaluate the evolution and anthropic disturbance ingeothermal fields: The case of Los Azufres geothermal field, México. Revista Mexicana de Ciencias Geológicas, 27, 3, 2010, p. 520-529.

NIST Standard Reference Database 23: Reference Fluid Thermodynamic and Transport Properties-REFPROP, Version 9.1, National Institute of Standards and Technology, Standard Reference Data Program, Gaithersburg, Maryland, 2013.

Rosi M, Sbrana A, (1987). Phlegrean Fields: petrography. Quad. Ric. Sci. 114, 60–79.

Taleghani AD: An improved closed-loop heat extraction method for geothermal resources. Journal of Energy resources Technology, ASME, December 2013, 135 (4), doi: 10.1115/1.4023175

Templeton JD, Ghoreishi-Madiseh SA, Hassani F, Al-Khawaja MJ: Abandoned petroleum wells as sustainable sources of geothermal. Energy 2014, 70: 366–373.

VV.AA, The Future of Geothermal Energy e Impact of Enhanced Geothermal System (EGS) on the United States in the 21th Century, MIT-Massachusetts Institute of Technology, USA, 2006.

Wang Z, McClure MW, Horne RN: A single-well EGS configuration using a thermosiphon. Proceedings of Thirty-Fourth Workshop on Geothermal Reservoir Engineering Stanford University, Stanford, California, February 9-11, 2009.

Wight NM, Bennett NS: Geothermal energy from abandoned oil and gas wells using water in combination with a closed wellbore. Applied Thermal Energy 2015, 89: 908-915.

Yari M: Exergetic analysis of various types of geothermal power plants. Renewable Energy 35 (2010) 112–121.

Xiang J Y, Cali M, and Santarelli M, 2004: Calculation for Physical and Chemical Exergy of Flows in Systems Elaborating Mixed-phase Flows and a Case Study in an IRSOFC Plant. Int. J. Energy Res., 28, pp. 101–115.

Zarrouk SJ, Moon H: Efficiency of geothermal power plants: A worldwide review. Geothermics 2014, 51, 142–153.

Zollo A, Maercklin N, Vassallo M, Dello Iacono D, Virieux J and Gasparini P, (2008). Seismic reflections reveal a massive melt layer feeding Campi Flegrei caldera, Geophys.Res.Lett., 35, L12306, doi:10.1029/2008GL03424.

Acknowledgements

The authors declare that they have no competing interests.

The authors declare that no other contributors have provided technical or writing assistance.

Appendix A: design of the dry cooling tower and evaluation of fans power

Appendix nomenclature

$A_{a,ch}$	heat exchanger surface of a single air channel, [m^2]
$D_{a,ch}$	equivalent diameter of air channels, [m]

$D_{w,i}$	inner diameter of the coil duct, [m]
$D_{w,o}$	outer diameter of the coil duct, [m]
ΔP_a	Pressure loss across the fin-tube heat exchanger, [Pa]
η_f	single fin efficiency
η_r	overall finned surface efficiency
$H = N_{ppr} * t_h$	total height of the fin-tube heat exchanger, [m]
$L = N_R * t_l$	total length of the fin-tube heat exchanger, [m]
LMTD	Logarithmic mean temperature difference, [K]
λ_c	thermal conductivity of the finned coil material, [W/(m K)]
$\dot{m}_a$	total air flow rate across the fin-tube heat exchanger, [kg/s]
ψ	effective porosity of the fin-tube heat exchanger
μ_a	dynamic viscosity of air, [Pa s]
$N_f = N_p W/t_r$	total number of fins
$N_p = N_{ppr} * N_R$	total number of pipes
N_{ppr}	pipes per row
N_R	rows number
ξ	pressure drop coefficient
Pr_a	Prandtl number of air
ρ_a	density of air, [kg/m^3]
$Re_{Da,ch}$	Reynolds number of air referred to the equivalent diameter of channels
s_r	fin width, [m]
T_a	Air temperature, [K or °C]
T_{CT}	Water temperature, [K or °C]
t_h	space between two consecutive pipes the same row, [m]
t_l	space between two rows, [m]
t_r	fin spacing, [m]
$(UA)_{tot}$	Product of the overall heat transfer coefficient and finned surface, [W/K]
$V_{a,ch}$	volume of a single air channel

W	total width of the fin-tube heat exchanger, [m]
w_a	frontal velocity of the air, [m/s]
$w_{a,m}$	mean gas velocity in the air channel, [m/s]

The fin-tube heat exchanger geometry of the dry cooling tower was optimized to minimize the fan power at the given heat flow rate at the condenser unit. The Figure A1 shows the reference geometry for the coil and the fluid path, namely a staggered tube arrangement with a parallel flow configuration. The optimization algorithm chooses the best values of W, H, and L which allow the required heat transfer with the minimum pressure losses. The mathematical form of the optimization problem reads:

$$\min_{W;H;L}\left[\frac{\dot{m}_a \Delta P_a}{\rho_a}\frac{1}{\eta_{em,fan}}\right] \qquad (A.1)$$

where:

$$\Delta P_a = \xi \frac{L}{D_{a,ch}} \rho_a \frac{w_{a,m}^2}{2} \qquad (A.2)$$

subject to:

$$T_{a,out} - T_{a,in} = 10\ K \qquad (A.3)$$

$$T_{wCT,out} - T_{a,in} = 5\ K \qquad (A.4)$$

$$\dot{m}_a = w_a \rho_a WH \qquad (A.5)$$

$$Re_{D_{a,ch}} > 800 \qquad (A.6)$$

$$\dot{m}_{wCT}\left(h_{1,wCT} - h_{3,wCT}\right) = \dot{m}_a c_a \left(T_{a,out} - T_{a,in}\right) = (UA)_{tot} LMTD \qquad (A.7)$$

The following ancillary equations apply:

$$LMTD = \frac{\left(T_{wCT,in} - T_{a,out}\right) - \left(T_{wCT,out} - T_{a,in}\right)}{\ln\left(\frac{T_{wCT,in} - T_{a,out}}{T_{wCT,out} - T_{a,in}}\right)} \qquad (A.8)$$

$$T_{a,in} = T_a \quad T_{wCT,in} = T_{1,wCT} \quad T_{wCT,out} = T_{3,wCT} \qquad (A.9)$$

$$(UA)_{tot} = N_{PPR}\left(\frac{1}{k_w\left(D_{w,i}\pi\right)(WN_R)} + \frac{\ln\left(\frac{D_{w,o}}{D_{w,i}}\right)}{2\pi\lambda_c(WN_R)} + \frac{1}{k_a\left(\frac{A_{a,ch}N_f}{N_{ppr}}\right)\eta_r}\right)^{-1} \qquad (A.10)$$

The fixed geometrical parameters, t_h, t_l, t_r,s_r are shown in Table A1. The pressure drop coefficient, ξ, was evaluated according to the correlation presented in (Branislav et al., 2006), namely:

$$\xi = \left(0.52 + \frac{180}{Re_{D_{a,ch}}^{0.85}}\right)\left(\frac{A_{a,ch}}{(t_h - D_{w,o})(t_r - s_r)}\right)^{-0.7}\left(\frac{2(X_D - D_{w,o})}{t_h - D_{w,o}}\right)^{0.65} \qquad (A.11)$$

The Figure A2 shows the single flow channel (highlighted in red). The characteristic length of the convective process is the hydraulic diameter of the air channel, namely:

$$D_{a,ch} = 4V_{a,ch}\psi/A_{a,ch} \qquad \text{(A.12)}$$

where

$$V_{a,ch} = t_h t_l (t_r - s_r) \quad A_{a,ch} = D_{w,o}\pi(t_r - s_r) + 2\left(t_h t_l - \frac{D_{w,o}^2\pi}{4}\right) \qquad \text{(A.13)}$$

$$\psi = 1 - \frac{s_r}{t_r} - \frac{\pi D_{w,o}^2 (t_r - s_r)}{4 t_h t_l t_r} \qquad \text{(A.14)}$$

$V_{a,ch}$ is the volume of a single air channel between two consecutive rows, $A_{a,ch}$ is the corresponding heat exchanging surface made of the two lateral fins and the two above and below half-coils, ψ is the so-called *porosity* and represents the void fraction of the finned coil. According to (Frass et al., 2015), the Nusselt number can be evaluated as:

$$Nu_a = C_1 Re_{D_{a,ch}}^{0.625} Pr_a^{1/3} \left(\frac{D_{a,ch}}{t_l}\right)^{1/3} \qquad \text{(A.15)}$$

where $Re_{D_{ch}}$ is evaluated through the mean gas velocity, $w_{a,m}$, given by the frontal velocity, $w_{a,in}$, divided by the porosity ψ, namely:

$$w_a = \frac{\dot{m}_a}{\rho_a WH} \qquad w_{a,m} = \frac{\dot{m}_a}{\rho_a WH} \qquad Re_{D_{a,ch}} = \rho_{a,} w_{a,m} D_{a,ch}/\mu_a \qquad \text{(A.16)}$$

Air thermo-physical properties are evaluated at the average temperature between the inlet and outlet sections. We used a value of $C_1 = 0.24$ as suggested in (Frass et al., 2015) for staggered tube arrangements.

The convective heat transfer coefficient within the ducts (water side), h_w, was evaluated through the classical Dittus-Boelter equation for turbulent flow (Lavine et al. 2001). The thermo-physical properties of the water were evaluated at the mean temperature between the inlet and outlet sections.

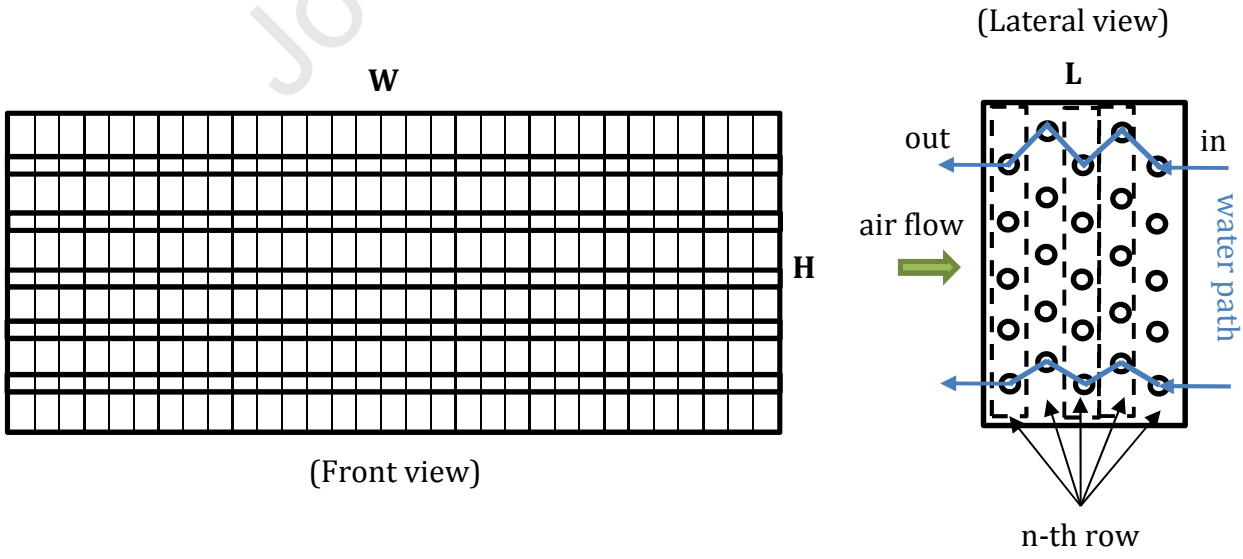

Fig. A1: Front and lateral view of the fin-tube heat exchanger.

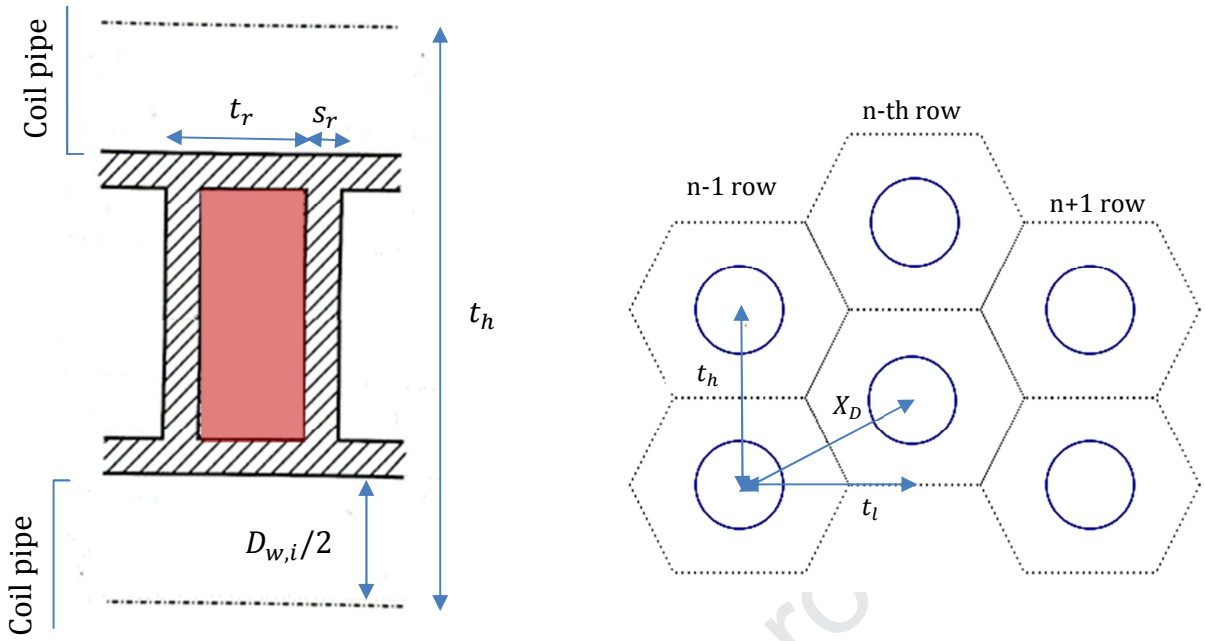

(a) (b)

Figure A2: (a) air channel between two consecutive fins and water duct; (b) hexagonal fin cells around each tube.

Fin efficiency, η_r, is evaluated as proposed in (Hong and Webb, 1996) for the hexagonal geometry of staggered tube configurations (see Fig. A2-b).

$$\eta_r = 1 - \frac{A_{a,ch} - 2\left(t_h t_l - \frac{\pi D_{w,o}^2}{4}\right)}{A_{a,ch}}\left(1 - \eta_f\right) \quad \text{(A.17)}$$

$$\eta_f = \frac{\tanh(mr\phi)}{mr\phi}\cos(0.1mr\phi) \quad \text{(A.18)}$$

$$\phi = \left(\frac{r_f}{r} - 1\right)\left[1 + \left(0.3 + \left(\frac{mr\left(\frac{r_f}{r} - r\right)}{2.5}\right)^{1.5 + \frac{1}{12}\frac{r_f}{r}}\left(0.26\left(\frac{r_f}{r}\right)^{0.3} - 0.3\right)\right)\ln\left(\frac{r_f}{r}\right)\right] \quad \text{(A.19)}$$

where $\frac{r_f}{r}$ is the effective radius ratio given by:

$$\frac{r_f}{r} = 1.27\frac{X_T}{r}\sqrt{\frac{X_D}{X_T} - 0.3} \qquad X_T = t_h/2 \qquad X_D = \frac{\sqrt{t_l^2 + \frac{t_h^2}{4}}}{2} \qquad r = \frac{D_{w,o}}{2} \qquad m = \sqrt{\frac{2k_a}{\lambda_c s_r}} \quad \text{(A.20)}$$

Table A1 – Geometry and operative parameters of the fin-tube heat exchanger given by the optimization procedure

Parameter	Value	Unit
Heat exchanger geometry		
W	10.93	m
H	0.50	m
L	2.25	m
Volume (WxHxL)	12.29	m^3
Frontal area (WxH)	24.58	m^2

ψ	0.76	
N_{ppr}	25	
N_R	10	
t_h	5.00×10^{-2}	m
t_l	5.00×10^{-2}	m
t_r	5.00×10^{-3}	m
s_r	5.00×10^{-4}	m
Thermal conductivity of the fin-tube heat exchanger	200	W/(m K)
η_f	0.92	
$D_{a,ch}$	7.55×10^{-3}	m
$D_{w,o}$	2.20×10^{-2}	m
$D_{w,i}$	1.80×10^{-3}	m
Operative condition - air side		
Reynolds Number	934	
Prandtl number	0.72	
Nusselt Number	8.28	
Convective heat transfer coefficient, k_a	28.37	W/(m^2 K)
Friction factor	0.55	
Operative condition - water side		
Reynolds number	2.51×10^4	
Prandtl number	5.08	
Nusselt number	123.96	
Convective heat transfer coefficient, k_w	4.26×10^3	W/(m^{2}K)

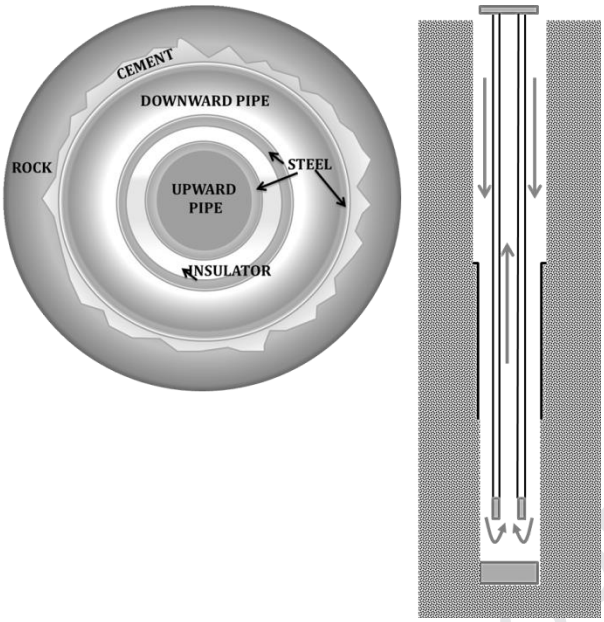

Figure 1 – The wellBore Heat eXchanger.

Figure 2 - Campi Flegrei caldera (Carlino et al., 2012)

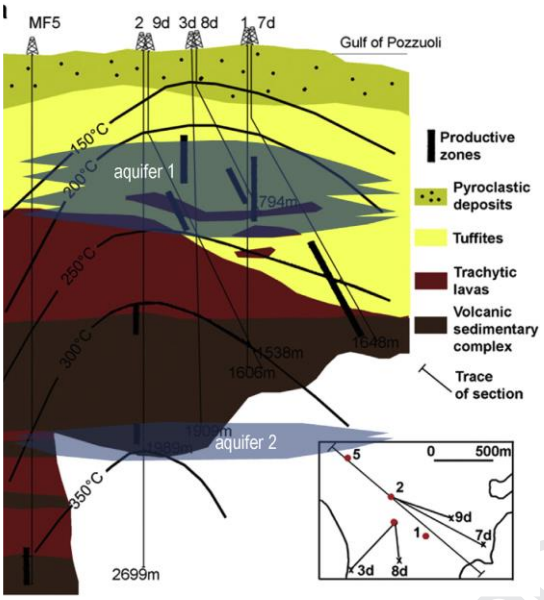

Figure 3 – Model of geothermal reservoir and acquifers (Carlino et al., 2016).

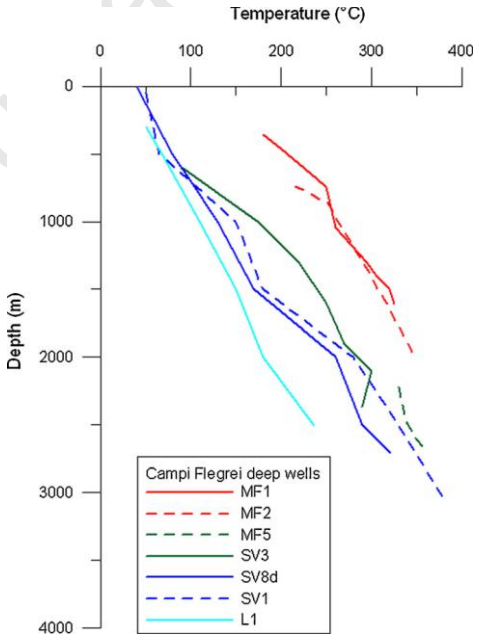

Figure 4 - Temperature profiles of Campi Flegrei deep wells (AGIP, 1987; Carlino et al. 2012).

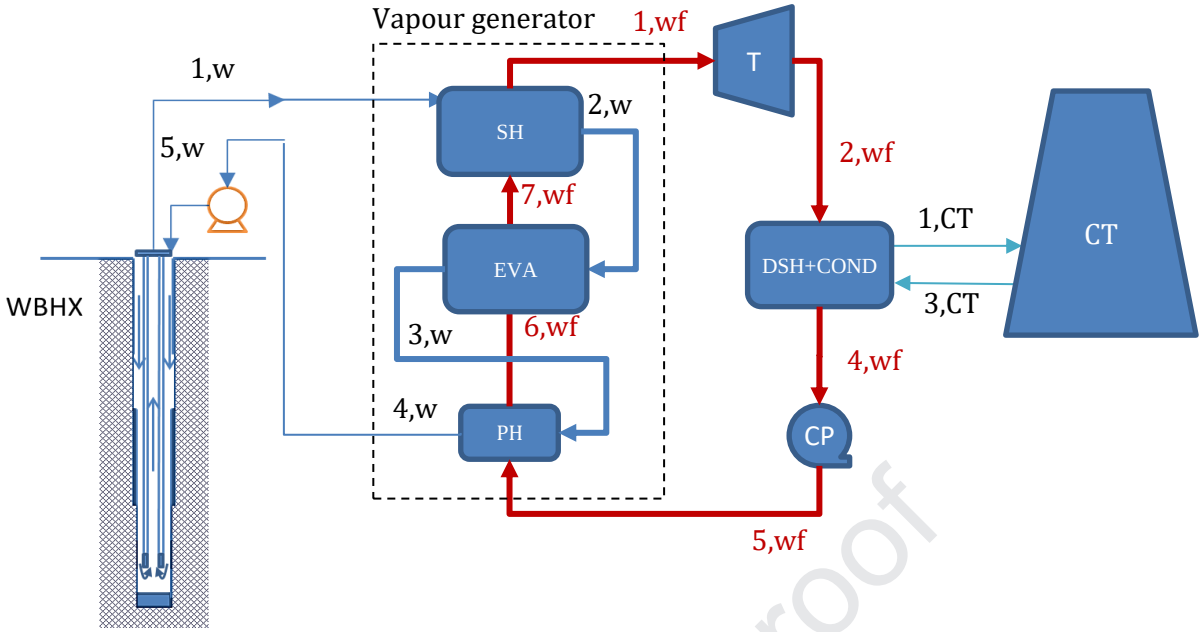

Figure 5 - Scheme of the analyzed WBHX – ORC system.

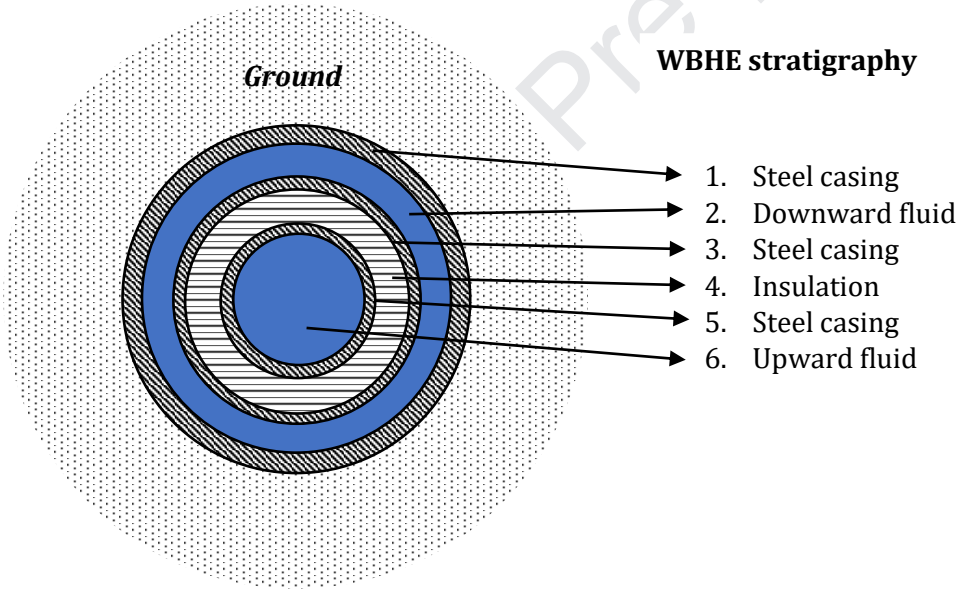

Figure 6 - WBHE axial section A-A.

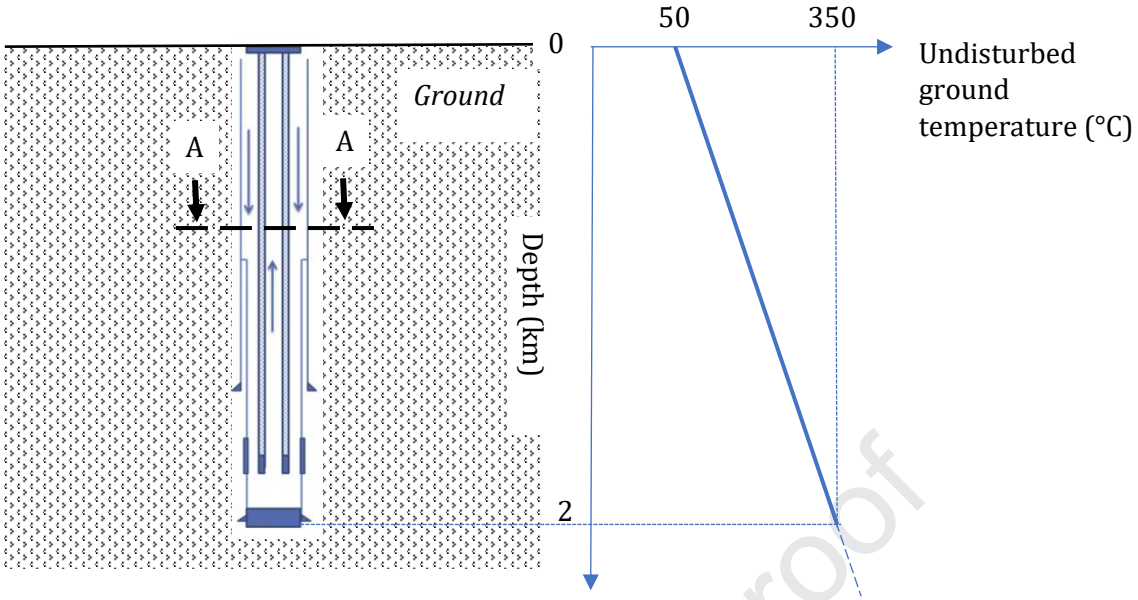

Figure 7 - Vertical section of the WBHX and temperature profile of the undisturbed ground.

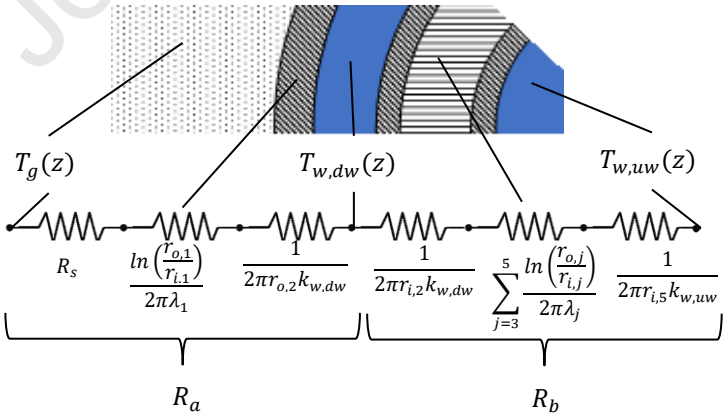

Figure 8 - WBHX thermal resistance model.

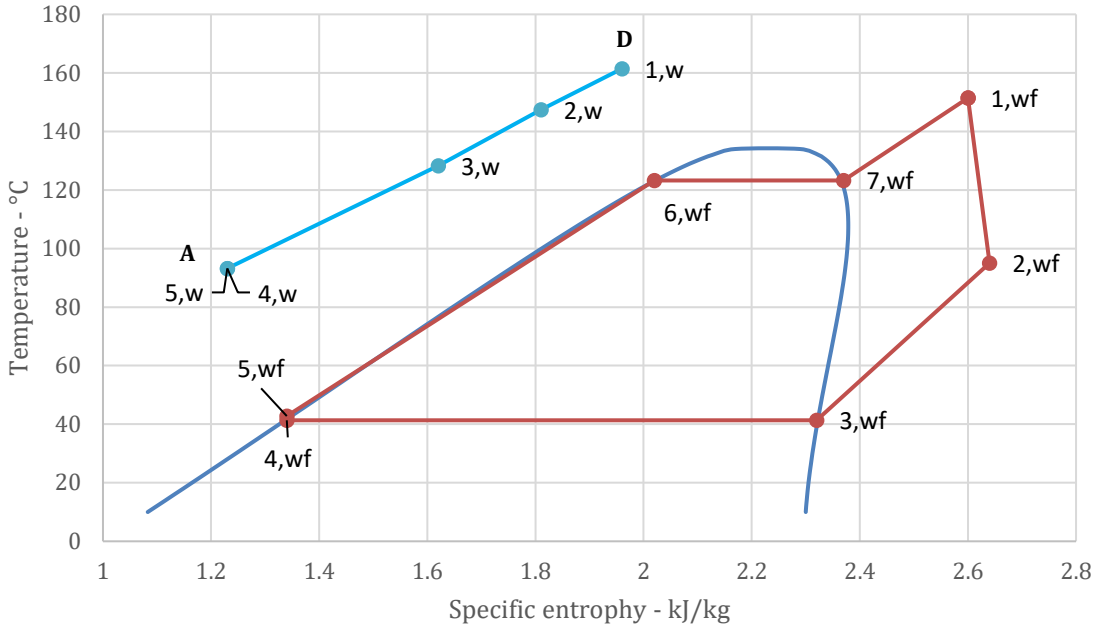

Figure 9 - TS diagram of the ORC

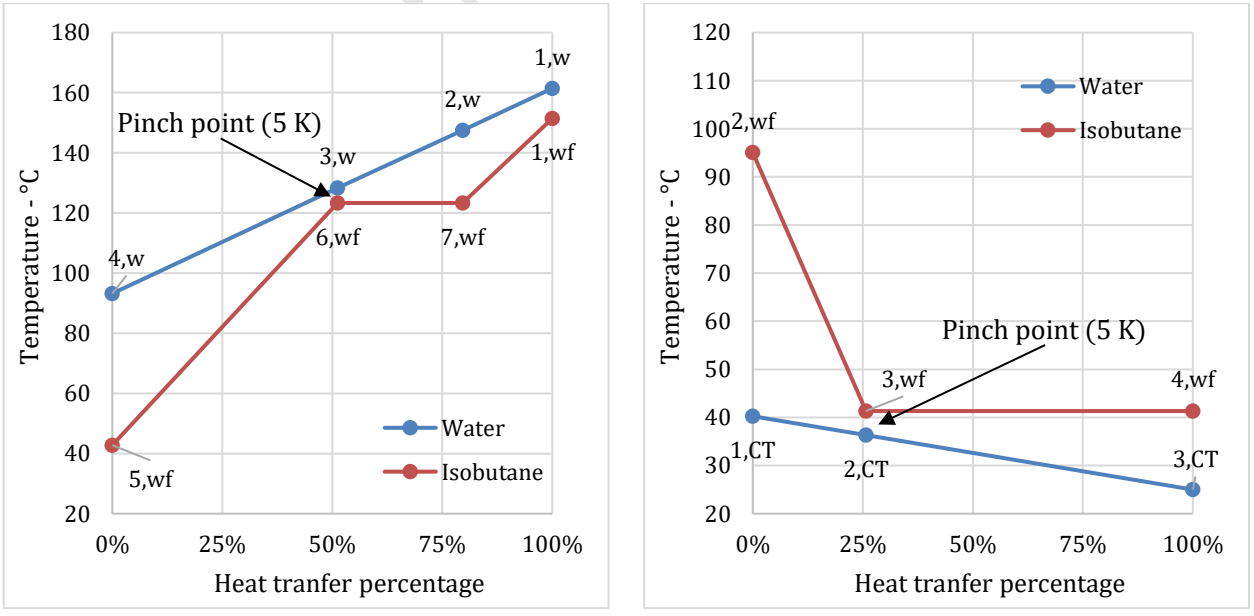

Figure 10 - Heat transfer vs temperature charts for the vapour generator (left) and desuperheater-condenser (right).

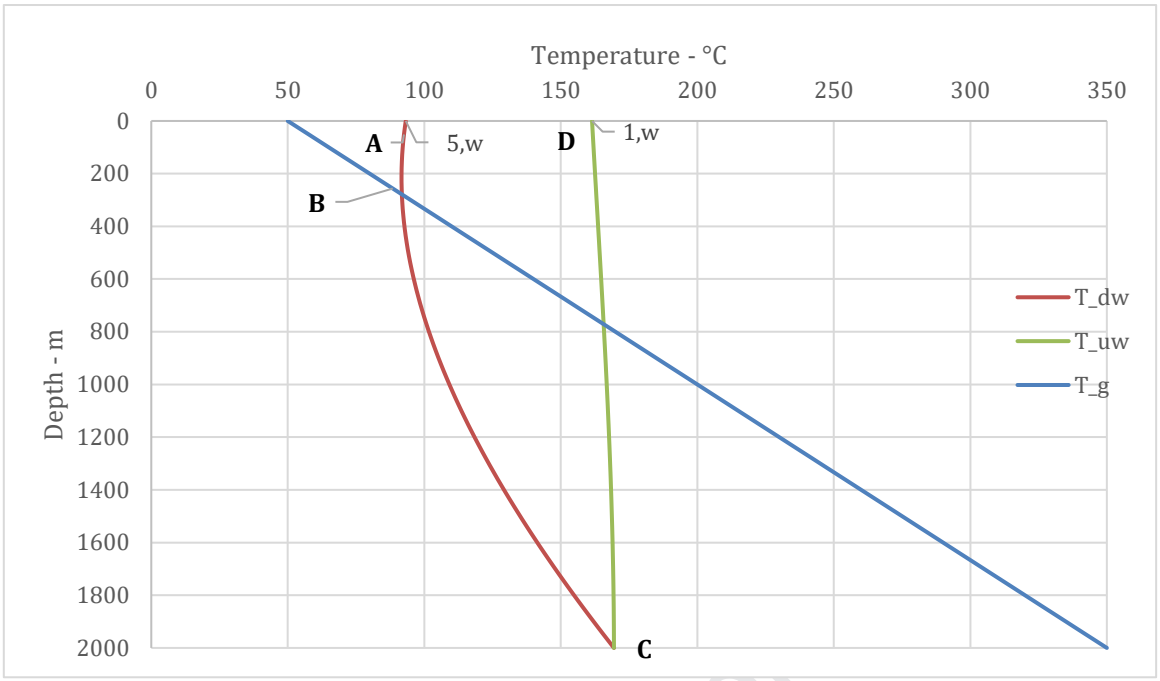

Figure 11- Temperature profiles along the WBHX.

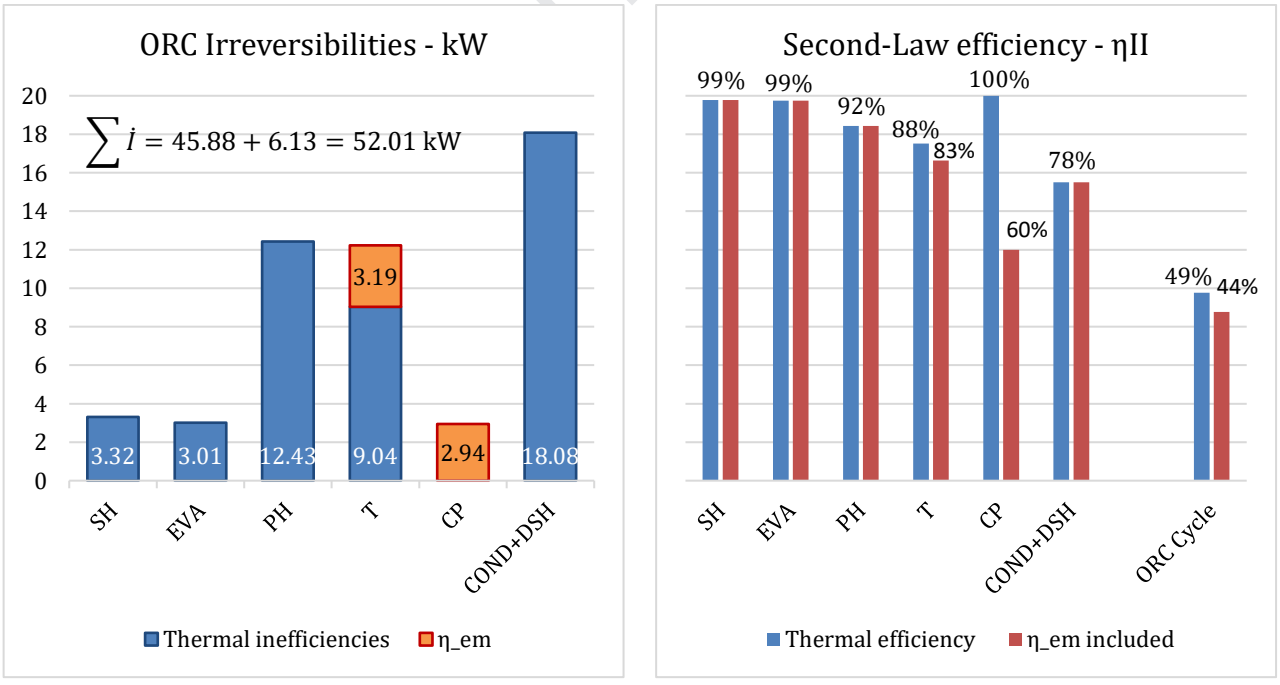

Figure 12 – Irreversibilities (a) and Second-Law efficiency (b) values for each ORC component

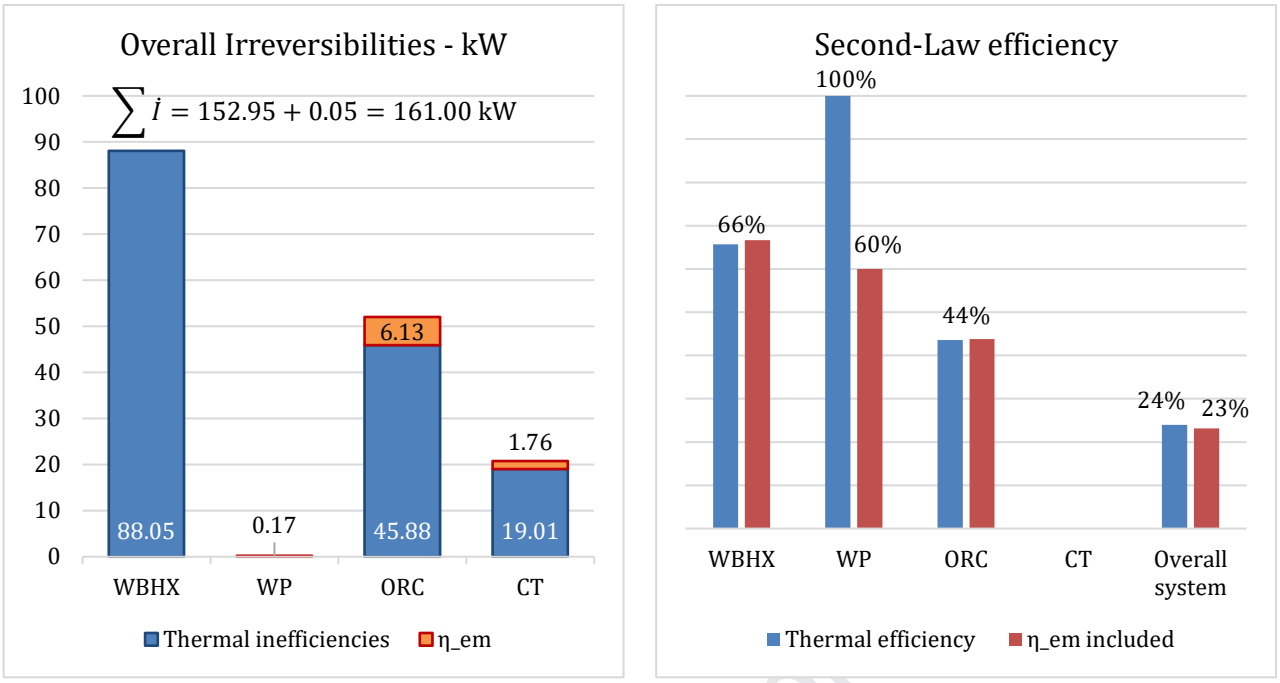

Figure 13 – Irreversibilities (a) and Second-Law efficiency (b) values for the main components of the overall system

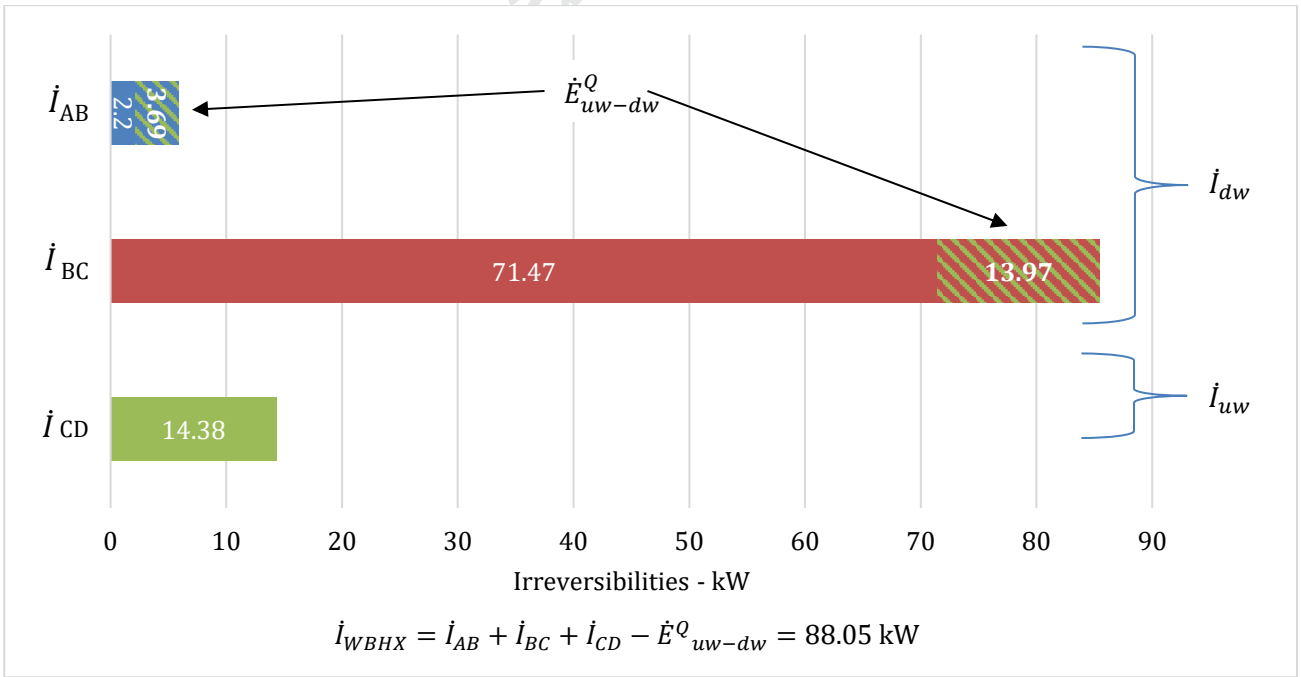

Figure 14 - Irreversibility production rates within the WBHX. The dashed areas correspond to the exergy losses due to the shorth-circuit heat transfer between the upward and downward ducts.

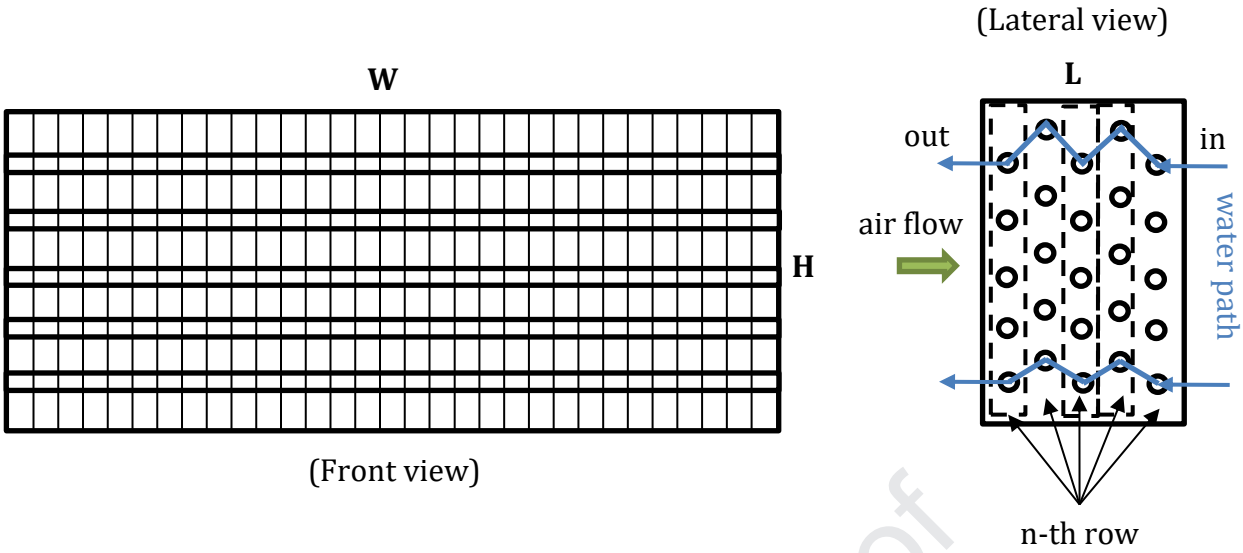

Fig. A1: Front and lateral view of the fin-tube heat exchanger.

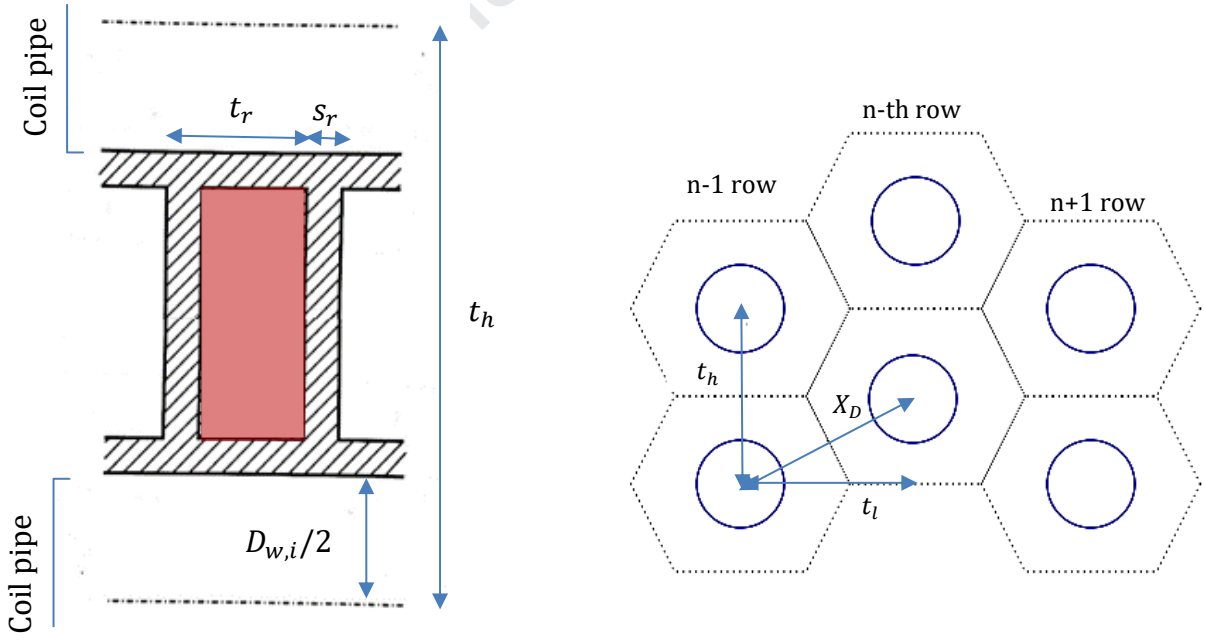

(a) (b)

Figure A2: (a) air channel between two consecutive fins and water duct; (b) hexagonal fin cells around each tube.

HIGHLIGHTS

- The paper presents studies and applications of the WellBore Heat eXchanger
- We present a comprehensive energy and exergy analysis of a WBHX – ORC system
- The analysis includes the cooling system and the geothermal source response
- Results show the main components and design parameters affecting WBHX efficiency
- The proposed methodology has been applied to a case study in Campi Flegrei (Italy)

Declaration of interests

☒ The authors declare that they have no known competing financial interests or personal relationships that could have appeared to influence the work reported in this paper.

☐The authors declare the following financial interests/personal relationships which may be considered as potential competing interests: